10-1-2017

Distribution and female reproductive state differences in orexigenic and anorexigenic neurons in the brain of the mouth brooding African cichlid fish, Astatotilapia burtoni

Danielle T. Porter
Louisiana State University

David A. Roberts
Louisiana State University

Karen P. Maruska
Louisiana State University

Recommended Citation

Porter, D., Roberts, D., & Maruska, K. (2017). Distribution and female reproductive state differences in orexigenic and anorexigenic neurons in the brain of the mouth brooding African cichlid fish, Astatotilapia burtoni. *Journal of Comparative Neurology, 525* (14), 3126-3157. https://doi.org/10.1002/cne.24268

Distribution and Female Reproductive State Differences in Orexigenic and Anorexigenic Neurons in the Brain of the Mouth brooding African Cichlid Fish, *Astatotilapia burtoni*

Authors: Danielle T. Porter, David A. Roberts, and Karen P. Maruska*

Affiliation: Department of Biological Sciences, 202 Life Sciences Bldg., Louisiana State University, Baton Rouge, LA. 70803

**Corresponding author:* Email: kmaruska@lsu.edu; Phone: 225-578-1738

Abbreviated title: Orexigenic and anorexigenic neurons in female cichlid brain

Associate Editor: Thomas E. Finger

Key words: AGRP; CART; feeding; lateral tuberal nucleus; NPY; parental care; POMC; reproduction; teleost; RRID:AB_2313606; RRID:AB_2336819; RRID:AB_2336382; RRID:AB_514497; RRID:SCR_014329; RRID:SCR_014199

Support and grant sponsors: Support was provided by startup funds from the College of Science and Department of Biological Sciences at Louisiana State University (KPM), a Ralph E. Powe Faculty Enhancement Award from Oak Ridge Associated Universities (KPM), grants in aid of research from Sigma Xi Scientific Society and LSU Chapter of Sigma Xi (DTP), and the National Science Foundation (IOS-1456558 and IOS-1456004 to KPM).

ABSTRACT

Integration of reproduction and metabolism is necessary for species survival. While the neural circuits controlling energy homeostasis are well-characterized, the signals controlling the relay of nutritional information to the reproductive axis are less understood. The cichlid fish *Astatotilapia burtoni* is ideal for studying the neural regulation of feeding and reproduction because females cycle between a feeding gravid state and a period of forced starvation while they brood developing young inside their mouths. To test the hypothesis that candidate neuropeptide-containing neurons known to be involved in feeding and energy homeostasis in mammals show conserved distribution patterns, we performed immunohistochemistry and *in situ* hybridization to localize appetite-stimulating (neuropeptide Y, NPY; agouti-related protein, AGRP) and appetite-inhibiting (cocaine and amphetamine-regulated transcript, CART; pro-opiomelanocortin, *pomc1a*) neurons in the brain. NPY, AGRP, CART, and *pomc1a* somata showed distribution patterns similar to other teleosts, which included localization to the lateral tuberal nucleus (NLT), the putative homolog of the mammalian arcuate nucleus. Gravid females also had larger NPY and AGRP neurons in the NLT compared to brooding females, but brooding females had larger *pomc1a* neurons compared to gravid females. Hypothalamic *agrp* mRNA levels were also higher in gravid compared to brooding females. Thus, larger appetite-stimulating neurons (NPY, AGRP) likely promote feeding while females are gravid, while larger *pomc1a* neurons may act as a signal to inhibit food intake during mouth brooding. Collectively, our data suggest a potential role for NPY, AGRP, POMC and CART in regulating energetic status in *A. burtoni* females during varying metabolic and reproductive demands.

INTRODUCTION

Reproduction in vertebrates is an energetically costly process, especially for females who invest in egg production and parental care (Clutton-Brock & Vincent, 1991; Grone, Carpenter, Lee, Maruska, & Fernald, 2012). Feeding and reproduction are tightly linked in most animals, and individuals must constantly sense and integrate cues from both the internal body and the external environment to make critical decisions about when to eat and when to reproduce. The brain plays a crucial role in maintaining these motivationally-driven behaviors as well as homeostatic behaviors such as food intake and body weight (Sohn, Elmquist, & Williams, 2013). Little is known, however, about which hormones and neurochemicals are involved in the complex regulation of feeding and reproduction, particularly in fishes, the largest and most diverse group of vertebrates with over 30,000 species.

Integration of reproduction and metabolism is an essential process for the survival and persistence of a species and is linked through evolutionary processes (Roa, 2013; Schneider, 2004). During reproductive periods, energy is diverted to maintain fertility, pregnancy, and nursing (Roa, 2013; Wade & Jones, 2004). Reproduction is energetically costly, however, and during unfavorable conditions (e.g., famine, pathological conditions) the body must prioritize physiological processes essential for survival (Wade & Jones, 2004). Changes in energy stores result in the fluctuation of metabolic hormones (e.g., ghrelin, insulin, leptin), nutritional signals (e.g., glucose, lipids), and neuropeptides (e.g., Neuropeptide Y, NPY; Pro-opiomelanocortin, POMC; Agouti-related protein, AGRP; cocaine- and amphetamine-regulated transcript, CART) that regulate metabolism and fertility through interaction with the hypothalamic-

pituitary-gonadal (HPG) axis (Roa, 2013; Shahjahan, Kitahashi, & Parhar, 2014). While the neural circuits controlling energy homeostasis are relatively well-characterized in mammals (Roa, 2013), the signals controlling and modulating the relay of nutritional status to the reproductive axis are not well understood in any vertebrate.

The integrative processes that regulate reproduction and metabolism are controlled by hormones and neuropeptides in the brain (Daniel, Foradori, Whitlock, & Sartin, 2013; Navarro & Kaiser, 2013; Roa, 2013; Tena-Sempere, 2007). While there are exceptions, many of the molecules that promote feeding also inhibit the reproductive system and vice versa (Schneider, 2004). For example, in mammals, feeding signals can stimulate the reproductive axis by promoting the release of gonadotropin-releasing hormone (GnRH) from the hypothalamus, and luteinizing hormone (LH) and follicle-stimulating hormone (FSH) from the pituitary to promote steroid synthesis and gamete production (Copeland, Duff, Liu, Prokop, & Londraville, 2011). However, some feeding signals, such as ghrelin (a peptide hormone typically produced by the gastrointestinal tract to stimulate hunger and feeding), inhibit the reproductive axis by suppressing the release of LH (Tena-Sempere, 2007) and the activity of the melanocortin system (Schioth & Watanobe, 2002; Tena-Sempere, 2007; Yang, Atasoy, Su, & Sternson, 2011). The melanocortin system plays an important role in the hypothalamic regulation of energy balance, and encompasses melanocyte-stimulating hormone (MSH), adrenocorticotrophic hormone (ACTH), AGRP, and the central melanocortin 3 (MC3) and 4 (MC4) receptors (Schioth & Watanobe, 2002). In teleost fishes, much like mammals, the reproductive axis is tightly connected with energy balance. For instance, the central melanocortin system in teleosts functions similarly to mammals in that up-

regulation of the melanocortin receptor antagonist, AGRP, occurs during fasting in goldfish (Cerda-Reverter & Peter, 2003) and zebrafish (Song, Golling, Thacker, & Cone, 2003). The melanocortin system, more specifically the melanocortin 4 receptor, is also involved in the regulation of growth and reproductive hormones in zebrafish (Zhang, Forlano, & Cone, 2012). Thus, it appears that at least some of the neural control mechanisms regulating energetics and reproduction, including the melanocortin system, are conserved across vertebrates.

Metabolic status also acts to regulate the production of neuropeptides to either promote or inhibit feeding behavior (Williams & Elmquist, 2012). In mammals, the arcuate nucleus of the hypothalamus is one of the best-studied brain regions for the neural control of feeding and appetite (Sohn et al., 2013). POMC, AGRP, and NPY neurons are all found in the arcuate nucleus and are key regulators of food intake and energy expenditure (Kong et al., 2012). Yang et al. (2011) showed that the hormone leptin is involved in a "flip-flop" memory storage circuit with ghrelin (set signal), in which leptin (reset signal) inhibits orexigenic (appetite-stimulating) neurons expressing neuropeptides such as AGRP and NPY, and stimulates anorexigenic (appetite-suppressing) neurons expressing neuropeptides such as alpha-melanocyte stimulating hormone (α-MSH) and CART. POMC, NPY, AGRP, and CART are found in the lateral tuberal nucleus (NLT) of fishes, the putative homolog of the arcuate nucleus in mammals (Liu et al., 2010). Due to the structural homology of these neuropeptides across taxa (Hoskins & Volkoff, 2012), comparative studies on their distribution, function, and how they may change under varying reproductive and metabolic states in diverse taxa will contribute to our understanding of the evolution of the regulation of

feeding and energy expenditure.

The African cichlid fish *Astatotilapia burtoni* is an excellent system to investigate which neuropeptides are involved in the integration of feeding and reproduction because the females cycle between an energy investment state with increased food intake to promote ovarian recrudescence and vitellogenesis, followed by spawning and a brooding maternal care state when they consume little to no food. During this brooding starvation period, which typically lasts ~2 weeks in *A. burtoni*, there is a noticeable decrease in body mass and delays in ovarian cycles and subsequent spawning (Fernald & Hirata, 1979; Grone et al., 2012; Renn, Carleton, Magee, Nguyen, & Tanner, 2009). Thus, there are clear metabolic, physiological, and behavioral differences between the gravid (full of eggs) energy investment phase and the mouth brooding energy consumptive phase. Little is known, however, about potential involvement of feeding-relevant neuropeptides in the brain in regulating the cyclical transition between these divergent reproductive-energy investment states.

The purpose of this study was to test the hypothesis that the drastically different reproductive and energetic states of gravid and mouth brooding *A. burtoni* females are associated with changes in candidate orexigenic and anorexigenic neural systems. While we use the general terms orexigenic for AGRP and NPY, and anorexigenic for CART and *pomc1a*, it is important to recognize that these neuropeptides (and their respective genes) are also involved in many other functions across different brain regions. Specifically, we aimed to 1) map the distribution of candidate orexigenic (AGRP, NPY) and anorexigenic (CART) neurons in the brain for the first time in a mouth brooding fish species, and 2) quantify differences in somata sizes of AGRP-, NPY-, and

pomc1a-expressing neurons in NLT, as well as mRNA expression levels in the hypothalamus among divergent reproductive and energetic states.

MATERIALS AND METHODS

Animals

A laboratory stock of *Astatotilapia burtoni* (Günther 1894) derived from a wild-caught population originally collected from Lake Tanganyika, Africa were housed in community aquaria kept at conditions similar to their natural environment: pH 7.8-8.0, temperature 29-30°C and a 12 hour light: 12 hour dark cycle with full spectrum illumination and constant aeration. Aquaria contained gravel along the bottom and terra cotta pot halves that served as shelters and to facilitate the establishment and maintenance of territories by dominant males. Fish were fed cichlid flakes (AquaDine, Healdsburg, CA) each morning and supplemented with brine shrimp (Sally's Frozen Brine Shrimp, San Francisco, CA) twice a week. All experiments were performed in accordance with the recommendations and guidelines stated in the National Institutes of Health (NIH) Guide for the Care and Use of Laboratory Animals, 2011. Experimental protocols were approved by the Institutional Animal Care and Use Committee (IACUC) at Louisiana State University.

To test for reproductive state differences in neuropeptide-containing neurons in the brain, we sampled both gravid females and mouth brooding parental females. Gravid females were initially selected based on body shape (distended abdomen), and gonadal status was subsequently confirmed based on oocyte diameters and gonadosomatic index (GSI) (GSI=[(gonad mass/body mass)*100]). Brooding females

were collected 6-8 days after the onset of brooding, which is at or slightly past the mid-way point of their 12-14 day brooding period. Criteria were set for both gravid (GSI>5.0) and brooding (GSI<1.0; fry total length 5-10 mm) females to ensure that individuals within each group were of similar state. Individuals falling outside of these criteria were excluded from the dataset. Females were anesthetized in ice-cold fish tank water, sacrificed by rapid cervical transection between the hours of 8-10 am, and their body mass (BM), standard length (SL), liver mass (LM) and ovary mass (OM) were immediately measured. Once the ovaries were removed, the six largest oocytes were collected from the right ovary and the diameters of the long axis were measured and averaged. Liver mass was used to calculate the hepatosomatic index (HSI = [(liver mass/body mass)*100]) as a proxy for energy reserves, and ovary mass was used to calculate GSI as a measure of reproductive investment. Fulton's condition factor was also calculated using the formula $K=100(W/L^3)$ where W is the whole body mass in grams, L is the standard length in centimeters, and 100 is used to bring K close to 1. For brooding females, whole body mass without the presence of the brood in the buccal cavity was used to calculate K.

Immunohistochemistry

Throughout this paper, we use the following standard nomenclature for fishes when referring to mRNA and protein expression: lowercase and italicized names are used when referring to genes and mRNA expression measured via qPCR and *in situ* hybridization (ISH), while uppercase and non-italicized names are used when referring to proteins labeled by immunohistochemistry (IHC).

Following sacrifice by rapid cervical transection, brains were removed, fixed in 4% paraformaldehyde (PFA) in 1x phosphate buffered saline (PBS) overnight at 4°C, rinsed in PBS, and cryoprotected in 30% sucrose in 1xPBS at 4°C prior to sectioning. Cryoprotected brains were embedded in Optimal Cutting Temperature (OCT) compound (Tissue-Tek, Sakura Fine Tek, Torrance, CA) and sectioned in the transverse plane at 18 µm using a cryostat (Leica, CM1850). Sections were collected onto a series of four alternate slides (Superfrost Plus, VWR, Chicago, IL) so that all four candidate neuropeptides could be stained and analyzed in each individual brain. Additional brains used solely for peptide distribution were sectioned at 20 µm and collected on alternate slides. Slides were dried overnight at room temperature and stored prior to staining (4ºC for IHC; -80ºC for ISH).

To label NPY-, AGRP-, and CART-producing neurons in the brain, we performed standard immunohistochemistry. To minimize variability between individual IHC and ISH runs for quantification purposes, each staining experiment contained representatives of both gravid and brooding fish. Slides were brought to room temperature (20-22°C) and a hydrophobic barrier (Immedge pen; Vector Laboratories, Burlingame, CA) was applied around the sections and allowed to dry for about 40 minutes. The slides were then rinsed with 1xPBS (3x10 min) and non-specific binding was blocked (NPY: 2 hours; AGRP, CART: 1 hour) with 1xPBS containing 0.3%Triton-X-100 (Thermo-Scientific, Pittsburgh, PA), normal goat serum (NGS; Vector Laboratories) (NPY: 8%; AGRP: 2%; CART: 8%) and bovine serum albumin (BSA; Sigma-Aldrich, Atlanta, GA) (NPY: 1.0%; AGRP: 0.2%; CART: 0.2%). Slides were then incubated with primary antibody (AGRP: 1:10,000, H-003-53, Phoenix Pharmaceuticals, Burlingame, CA; CART: 1:5,000, H-003-

62, Phoenix Pharmaceuticals; NPY: 1:12,000, N9528, Sigma-Aldrich; all polyclonal made in rabbit) overnight (~16-18 hours) at 4°C in a sealed humidified chamber. The primary antibody incubation was followed by 1xPBS washes (3x10min), incubation with a biotinylated goat anti-rabbit secondary antibody (Vector Laboratories, RRID:AB_2313606) made in 1xPBS with NGS (NPY: 20%; AGRP: 3.3%; CART: 8.3%) for 45min-1hr, washes with 1xPBS (3x10min), quenching of endogenous peroxidases with 1.5-3.0% hydrogen peroxide in 1xPBS for 10 min, washes in 1xPBS (3x10min), incubation with avidin–biotin–horseradish peroxidase complex (ABC Elite kit; Vector Laboratories, RRID:AB_2336819) (NPY: 1.5 hours; CART, AGRP: 2 hours), washes in 1xPBS (3x10min), and reacted with a 3,3'-diaminobenzidine (DAB) peroxidase substrate kit with nickel chloride intensification (Vector Laboratories, RRID:AB_2336382) for 3 min. Slides were then soaked in distilled water for 10 min to stop the reaction, dehydrated in an ethanol series (50%, 70%, 95%, 100%), cleared in xylene, and coverslipped with Cytoseal 60 mounting media (Richard-Allan Scientific, San Diego, CA).

Antibody characterization

Details of the primary antibodies used in this study are provided in **Table 1**. All of these antibodies have been used and validated previously in other fish species [e.g., (Forlano & Cone, 2007; Sakharkar, Singru, Sarkar, & Subhedar, 2005; Singru et al., 2007)] and are listed in the JCN antibody database. The NPY polyclonal antibody (N9528; Sigma-Aldrich) was produced in rabbit using synthetic porcine NPY conjugated to keyhole limpet hemocyanin (KLH) as the immunogen, and is supplied as delipidized

whole antiserum. The staining pattern in *A. burtoni* was consistent with previous localization results in other fishes (Cerda-Reverter et al., 2000; Gaikwad, Biju, Saha, & Subhedar, 2004; Sakharkar et al., 2005).

The AGRP polyclonal antibody (H-003-53; Phoenix Pharmaceuticals, Inc.) was produced against synthetic residues 83-132 of Human AGRP and made in rabbit. Manufacturer information shows 100% cross-reactivity with AGRP (83-132)-amide (Human) and AGRP form C-NH2 (Human), and 0% cross-reactivity with Leptin, Orexin, NPY, α-MSH, and CGRP. The localization pattern in *A. burtoni* was similar to that described for AGRP in zebrafish (Forlano & Cone, 2007).

The CART polyclonal antibody (H-003-62; Phoenix Pharmaceuticals, Inc.) was produced against synthetic residues 55-102 of CART (rat, mouse, bovine), and made in rabbit. Manufacturer information shows Western blot detection of a 5-kDa band in rat brain and 100% cross-reactivity with CART 55-102 (rat, mouse, bovine, and human), 71.8% cross-reactivity with CART 61-102 (human), 0.01% cross-reactivity with AGRP 83-132-NH2 (human), and 0% cross-reactivity with Leptin, NPY, α-MSH, Orexin, and MCH. The staining pattern in *A. burtoni* was consistent with previous localization results in zebrafish (Akash, Kaniganti, Tiwari, Subhedar, & Ghose, 2014; Mukherjee, Subhedar, & Ghose, 2012).

To test for antibody specificity in the cichlid brain tissue, we performed two different types of controls. First, we preabsorbed each antibody (anti-NPY, -AGRP, -CART) with its respective immunizing control peptide (NPY: 1.617 μM, Sigma-Aldrich, #N5017; CART 55-102 peptide fragment: 1.521 μM, Phoenix Pharmaceuticals, #003-62; AGRP 83-132 peptide fragment: 706.6 nM Phoenix Pharmaceuticals, #003-53) in

excess overnight at 4ºC prior to tissue application. These preabsorption controls eliminated all reaction products and resulted in no staining when run simultaneously with non-preabsorbed antibody (**Fig. 1**). Other procedural controls (omission of secondary antibody, ABC, and DAB) also resulted in no staining. Second, we performed *in situ* hybridization to label mRNA for *agrp* (N=2, SL=45.1±1.50 mm, BM=2.94±0.93 g, GSI=0.85±1.43), *npy* (N=5, SL=38.2±1.92 mm, BM=1.61±0.26 g, GSI=1.14±0.98), *cart2* (N=7, SL=39.0±6.4 mm, BM=1.91±0.64 g, GSI=2.19±2.38) and *cart4* (N=4, SL=39.3±6.8 mm, BM=1.86±0.44 g, GSI=3.13±2.62) (described below) on females of mixed reproductive states (**Figs. 1, 2**). We used ISH rather than western blots to more accurately compare it to the localization of different IHC-identified cell populations within sectioned brain tissue.

Staining of *agrp* mRNA in cells of the NLT was identical to that observed by AGRP antibody (**Fig. 2A,B**). However, the AGRP antibody also stained the large neurons of gTN, which were not labeled via ISH. This IHC label remained after preabsorption of the AGRP antibody with excess AGRP peptide, suggesting that it is cross-reactive binding to some non-AGRP substance, similar to that described in the zebrafish (Forlano & Cone, 2007).

For *npy*, while mRNA was primarily localized to all of the same regions labeled with the NPY antibody (**Fig. 2C,D**) (with the exception of weak to no label in DT and gTN neurons with ISH, but strong antibody label), there were also numerous additional cells labeled throughout the brain by ISH that were not detected by the antibody (e.g. ICL, Vs, PGZ, IO, SGn, SVn). Duplicate *npy* genes (*npya, npyb*) are identified in *A. burtoni* (Hu et al., 2016), and our *npy* ISH results likely represent the distribution of

npya. We chose to examine this form rather than the teleost-specific duplicate, *npyb,* because in the related Nile tilapia *O. niloticus*, *npya* is expressed at much higher levels in the brain compared to *npyb*, responds to changes in feeding conditions that are not evident in *npyb*, and intracranial injections stimulate food intake (Yan et al., 2017). Thus it is possible that the neurons labeled in DT and gTN with IHC in *A. burtoni* represent *npyb* populations.

Similarly, the cells labeled by the CART antibody were primarily localized to the same regions as either *cart2* or *cart4* mRNA, but there were also additional *cart2* and *cart4* cells not detected by the CART antibody, and a population of large midline cells in nMLF that stained with the antibody but not *cart2* or *cart4* ISH (**Fig. 2-E-H**). Six CART prohormones are identified in *A. burtoni* (Hu et al., 2016), and we chose to examine *cart2* and *cart4* because of their known roles in feeding and energy metabolism, and their widespread localization in the brain of zebrafish, including hypothalamic regions involved in metabolic regulation such as NLT (Akash et al., 2014).

Some possibilities for the differences in staining between IHC and ISH include variations in protein translation (i.e. turnover, or post-translational modifications), low levels of protein or mRNA not detected by each staining technique, binding characteristics between antigens and antibodies/probes, differences between mRNA transcription and peptide storage within cells, cross-reactivity of antibodies with related peptides, or labeling of different gene forms due to teleost whole genome duplication.

Synthesis of riboprobes for *in situ* hybridization

To identify *pomc1a*, *agrp*, *npy*, *cart2,* and *cart4* mRNA-containing neurons, we performed chromogenic-based *in situ* hybridization. To identify *pomc1a*-containing neurons, we performed ISH as a proxy for α-MSH. This approach was used because pilot experiments with several commercially available α-MSH antibodies failed to produce reliable staining. Following the teleost-specific whole genome duplication, three forms of *pomc* (*pomc1a, pomc1b* and *pomc2*) are identified in *A. burtoni* and their localization in the brain and pituitary of this species was previously described (Harris, Dijkstra, & Hofmann, 2014; Hu et al., 2016). We chose to quantify *pomc1a* neurons because phylogenetic analyses indicate that *pomc1a* is the homolog to the mammalian form responsible for the synthesis and cleavage of α-MSH in the pituitary in response to satiety signals (Amano et al., 2005).

To localize cells, we used a digoxigenin (DIG) *in situ* hybridization protocol with riboprobes. Primers for each candidate gene were designed from the *A. burtoni* sequences available in Genbank (**Table 2**) and then commercially synthesized (Life Technologies, Bethesda, MD). Templates for the riboprobes were generated by PCR (PCR Platinum SuperMix, Life Technologies) from whole brain *A. burtoni* cDNA using gene-specific primers. The reaction conditions were as follows: 95°C for 1 min, 40 cycles of: (95°C for 15sec, 55°C for 15sec, 72°C for 1 min), and 72°C for 1 min. Purified PCR products (MinElute PCR kit, Qiagen, Chatsworth, CA) were then used as the template in the transcription reaction to incorporate DIG-labeled nucleotides (DIG RNA-labeling mix, Roche, Nutley, NJ) into the nucleic acid sequence, followed by probe purification (GE Illustra Probe Quant G-50 microcolumns). Probes were transcribed

from the T3 polymerase transcription initiation sequence (aattaaccctcactaaaggg) that was added to the reverse (for anti-sense probes) or forward (for sense control probes) gene-specific primers. PCR products and final probes were checked on a 1% agarose gel and verified to be bands of the correct size. Probes were diluted with hybridization buffer and stored at -20°C.

In situ hybridization

Chromogenic-based *in situ* hybridization was performed as previously described (Butler & Maruska, 2016; Grone & Maruska, 2015; Maruska, Butler, Field, & Porter, 2017), and all solutions used during the protocol were RNase-free (0.25 µm filtered). Briefly, sections were brought to room temperature (20-22°C) and a hydrophobic barrier (Immedge pen, Vector Laboratories) was applied and allowed to dry for about 40 minutes. The slides were then washed in 1xPBS (3x5min), fixed in 4% PFA (20min), washed in 1xPBS (2x5min), permeabilized in proteinase K (10 µg/ml final concentration, 10 min), washed in 1xPBS (10 min), fixed in 4% PFA for 15 min, washed in 1xPBS (2X5min), rinsed in milliQ water (3 min), incubated in 0.1M triethanolamine-HCl (pH 8.0) with acetic anhydride to 0.25% volume (10 min), washed in 1xPBS (5 min), and incubated for 2.5 hours in pre-hybridization buffer at 60-65°C in a sealed humidified chamber. The pre-hybridization solution was removed, DIG-labeled anti-sense probe was added (sense probes with the T3 sequence added to the forward primer were also used as controls to test probe specificity; **Fig. 1**), and slides were covered with hybrislips (Life Technologies) to hybridize overnight (12-16 hours) at 60-65°C in a sealed humidified chamber. Following hybridization, the slides were washed at 60-65°C in pre-warmed 2X saline-sodium-citrate (SSC):50% formamide (2x30 min), 1:1 mixture

of 2XSSC: Maleic acid buffer with 0.1% Tween-20 (MABT) (2x15min), and MABT (2x10 min). Slides were then washed at room temperature with MABT (2x10 min) and non-specific binding was blocked with MABT containing 2% BSA for 3 hours. Slides were then incubated with alkaline phosphatase-conjugated anti-DIG Fab fragments (Roche, RRID:AB_514497) diluted 1:5,000 in blocking solution (MABT with 2% BSA) at 4°C overnight in a humidified chamber. Slides were then washed with MABT (3x30 min) at room temperature, incubated in alkaline phosphatase (AP) buffer (2x5min), developed for 2-5 hours with 4-nitro-blue tetrazolium chloride/ 5-bromo-4-chloro-3-indolyl-phosphate (NBT/BCIP, Roche) substrate solution at 37°C. Slides were then washed with 1xPBS (3x5min) to stop the reaction, fixed in 4% PFA (10 min), washed in 1xPBS (3x5min), and coverslipped with aqueous mounting media (Aqua-mount, Thermo-Scientific).

Quantification of somata size

To test for reproductive state differences in neuropeptide-expressing neurons, we performed blind unbiased measurements of somata sizes for NPY, AGRP, and *pomc1a* labeled neurons from transverse sections without knowledge of the SL, BM, GSI or reproductive state of the fish. Cell size was determined by measuring cell profile areas contained within NLTv, NLTi, and NLTm (**Fig. 3A-D**) from 10 randomly selected neurons for NPY (representing ~24% of all cells) and AGRP (~22% of cells), and 20 randomly selected neurons for *pomc1a* (~25% of cells) per individual. We did not measure CART-ir somata because we could not always identify clearly distinguishable cells in the NLT, primarily due to the proximity of these cells to the brain edge, which

made it difficult to accurately measure cell areas due to tissue folding, edge-effect staining, and accumulation of debris during staining protocols. Measurements were taken at a point where the labeled cell perimeter was easily discernible and a distinct nucleus was visible under the 40x objective lens. Somata areas for each neuropeptide-containing cell type were then averaged for each individual and within each reproductive state (gravid and mouth brooding) for statistical comparisons.

Imaging and analysis

To map the distribution patterns for neuropeptide-containing neurons in the brain, stained slides were visualized on a Nikon Eclipse Ni microscope and photographs were taken with a color digital camera (Nikon DS-Fi2) controlled by Nikon elements software (RRID:SCR_014329). Neuroanatomical regions and specific brain nuclei were identified using atlases and cytoarchitecture previously described in *A. burtoni* (Burmeister, Munshi, & Fernald, 2009; Maruska et al., 2017; Munchrath & Hofmann, 2010) as well as in other fish species (Imura et al., 2003; Munoz-Cueto, Sarasquete, Zohar, & Kah, 2001; Wullimann, Rupp, & Reichert, 1996). Images were sharpened, adjusted for contrast, brightness, and levels, and distracting artifacts removed with the clone tool in Photoshop CS6 (Adobe Systems, San Jose, CA.; RRID:SCR_014199). Neuropeptide distribution maps were created by tracing the outline of the left side of a representative cresyl-violet-stained coronal section along with relevant nuclei and neuroanatomical structures. The traces were then duplicated and flipped horizontally to create a mirror image for representation of a full coronal section, and then the locations of immunoreactive cells and fibers for each neuropeptide were marked on top of the

coronal section. Cells were defined as stated above, and immunoreactive fiber densities were defined as follows: few= 4 or less, low density= greater than 4 but less than 20, moderately dense= 21-45, and dense= greater than 45 in the field of view using a 40x objective lens.

Quantitative PCR (qPCR)

To examine the mRNA levels of the same neuropeptides quantified for somata size and distribution, as well as several other relevant genes, we performed qPCR on macro-dissected hypothalamic regions from a different set of females. Gravid (N=15) and mouth brooding (N=13) females were sacrificed as described above and the brains were macro-dissected to first divide the brain into the telencephalon, diencephalon and mesencephalon, and rhombencephalon (**Fig. 3E**). The diencephalon was then further dissected so that the hypothalamus (without pituitary gland) was removed and used for qPCR. The brain was macro-dissected in this fashion to focus on the NLT, where somata sizes were quantified in a different set of animals, but also included other diencephalic nuclei (e.g. ATn, NRL, NDILI, NRP, NCIL) known to be involved in feeding and reproduction. This approach also removed any NPY, AGRP, CART, and/or *pomc1a* populations in other brain regions such as the preoptic nuclei. The hypothalamic tissue was weighed (2-6 mg per individual), rapidly frozen on dry ice, and then immediately stored at −80°C until RNA isolations were performed.

Hypothalamic tissue was homogenized and total RNA was extracted following manufacturer's protocols (RNeasy Mini Plus Kit, Qiagen). RNA yields were calculated using spectrophotometric values to ensure that a consistent amount of RNA (250ng/µl)

was used as a template for cDNA synthesis (iScript, Bio-Rad, Hercules, CA). The resulting cDNA was then re-measured via spectrophotometry to check the quality, and then diluted 1:5 prior to qPCR. Primers for all genes of interest [*pomc1a , agrp, ghrelin receptor (ghs-r1), leptin receptor (lepr), cart2, cart4, npy*] were designed from *A. burtoni* sequences available in Genbank (**Table 2**) using PrimerQuest (Integrated DNA Technologies, Coralville, IA) and then commercially synthesized (Life Technologies). qPCR was performed on a CFX connect Real-Time system (Bio-Rad) with duplicate reaction volumes of 20 µL. Reaction parameters were as follows: 95°C for 30sec, 45 cycles of 95°C for 1sec and 60°C for 30sec, and 65°C for 5sec, followed by a melt curve analysis. Fluorescence thresholds for each sample were automatically measured (CFX Manager, BioRad) and then PCR Miner (Zhao & Fernald, 2005) was used to calculate cycle thresholds and reaction efficiencies for individual wells as described previously (Maruska, Becker, Neboori, & Fernald, 2013; Maruska, Levavi-Sivan, Biran, & Fernald, 2011; Maruska, Zhang, Neboori, & Fernald, 2013). This curve-fitting qPCR algorithm objectively calculates reaction efficiency and the fractional cycle number at threshold (CT) of the amplification curve for more accurate computation of mRNA levels. The relative amount of mRNA was then normalized to the geometric mean of the two reference genes *18s* rRNA and *rpl32* (60S ribosomal protein L32) using the following equation: relative target mRNA levels = $[1/(1+E_{target})^{CT_{target}}] / [1/(1+E_{geomean})^{CT_{geomean}}] \times 100$, where E is the reaction efficiency and CT is the average cycle threshold of the duplicate reactions. Values of *18s* (Mann-Whitney; U=73.00; p=0.421) and *rpl32* (student's t-test; p=0.939; t=0.0771; df=25) did not differ between gravid and brooding females, indicating they are appropriate reference genes for this study. Normalizing the

mRNA levels to two reference genes, rather than one, allows for a more accurate quantification (Bustin, Benes, Nolan, & Pfaffl, 2005; Mitter et al., 2009).

Statistical analyses

To test for differences between reproductive states in physiological variables (GSI, HSI, oocyte diameter, SL, BM) we used two-tailed unpaired t-tests or non-parametric Mann-Whitney tests when assumptions of normality and equal variance were not met (SigmaPlot, Systat, Inc., San Jose, CA). Pearson Product Moment Correlations were used to test for correlations between GSI and somata sizes (compared between each peptide), HSI and somata sizes, and between different somata sizes. To account for positive relationships between somata size and body size, we compared gravid and brooding somata sizes with analysis of covariance (ANCOVA), using standard length (for somata size comparisons) or hypothalamic mass (for mRNA level comparisons) as a covariate. Statistical significance was set at P=0.05 for all comparisons. Bonferroni corrections or other similar procedures for multiple testing were not used because they reduce statistical power and increase the chance of type II errors, especially in small sample sizes. While these correction tests do reduce type I errors, their unacceptable effects on statistical power can mask potential biologically-relevant results and interpretations (Nakagawa, 2004).

RESULTS

Physiological differences between gravid and brooding females

A total of 24 female *A. burtoni* (12 gravid, 12 brooding) were used in this study for the physiological analysis, quantification of somata sizes, and IHC distribution of neuropeptides. Gravid females have higher GSI (Mann-Whitney; U=0.00; *P*<0.001) (**Fig. 4A**) and larger ova diameters (Student's t-test; *P*<0.001; t=17.614; df=22) (**Fig. 4B**) compared to brooding females. Gravid females also have higher HSI (Mann-Whitney; U=4.00; *P*<0.001) (**Fig. 4C**) and condition factors (Mann-Whitney; U= 25.00; *P*=0.013) (**Fig. 4D**) compared to brooding females, indicative of greater energy reserves.

Distribution of NPY, AGRP and CART neurons

Localization of NPY-immunoreactivity

Olfactory bulbs and telencephalon

NPY-ir cells occur in the ganglion of the terminal nerve (gTN) at the junction between the olfactory bulbs and rostral telencephalon (**Fig. 5, 6A**). In the olfactory bulbs, NPY-immunoreactive (-ir) fibers are present in the external cell layer (ECL), glomerular layer (GL), inner cell layer (ICL) and secondary olfactory layer (SOF) (**Fig. 5A**).

NPY-ir cells are essentially absent from dorsal telencephalic nuclei, with the exception of a few scattered cells in some regions of the central part of the dorsal telencephalon (Dc) (**Fig. 5D, 6B**). NPY-ir cells lie in several nuclei of the ventral telencephalon, including the lateral part of the ventral telencephalon (Vl) (**Fig. 5B-D, 6C**), rostral portion of the central part of the ventral telencephalon (Vc) (**Fig. 5B-C, 6C**),

ventral nucleus of the ventral telencephalon (Vv) (**Fig. 5B**), and a few small cells in the rostral subdivision of the dorsal part of the ventral telencephalon (Vd-r) (**Fig. 5C**).

NPY-ir fibers are abundant throughout the dorsal telencephalic regions (**Fig. 5A-F**). Low to moderately dense scattered NPY-ir fibers are present in the ventral part of the lateral zone of the dorsal telencephalon, subdivision 1 (Dl-v1), dorsal part of the lateral zone of the dorsal telencephalon (Dl-d), and medial part of the dorsal telencephalon, subdivision 1 (Dm-1) (**Fig. 5A-C**). Moderately dense NPY-ir fibers are present in the rostral ventral region of the lateral part of the dorsal telencephalon, subdivision 2 (Dl-v2) and density increased caudally in the Dl-v2 (**Fig. 5B-D**). Dense fibers lie in the nucleus taenia (NT) (**Fig. 5D**) and dorsal part of the dorsal telencephalon (Dd) (**Fig. 5D-F**). Dense fibers are also present in rostral sections of the ventral area of the central part of the dorsal telencephalon, subdivision 1 (Dc-1). In more caudal regions of Dc-1, fibers remain dense in the medial area, while fiber density decreases to moderate levels in the lateral area of Dc-1 (**Fig. 5B-C**). Moderately dense fibers are present in the unassigned subdivision of the dorsal telencephalon (Dx) (**Fig. 5B**), dorsal part of the dorsal telencephalon, dorsal subdivision (Dd-d) (**Fig. 5D-E**), medial part of the dorsal telencephalon, caudal subdivision 2 (Dm-2c) (**Fig. 5D**), medial part of the dorsal telencephalon, subdivision 3 (Dm-3) (**Fig. 5D-F**), central part of the dorsal telencephalon, subdivision 3 (Dc-3) (**Fig. 5D-F**), and granular zone of the lateral part of the dorsal telencephalon (Dl-g) (**Fig. 5C-E**). Low density fibers also lie in the medial part of the dorsal telencephalon, rostral subdivision 2 (Dm-2r) and central part of the dorsal telencephalon, subdivisions 4 (Dc-4) and 5 (Dc-5) (**Fig. 5D-E**).

Compared to dorsal telencephalic nuclei, NPY-immunoreactive fibers are less dense in ventral telencephalic nuclei, particularly the periventricular regions along the midline (**Fig. 5B-F**). Moderately dense NPY-ir fibers are present in the Vl (**Fig. 5B-D**), medial part of the supracommissural nucleus of the ventral telencephalon (Vs-m) (**Fig. 5D-F**), Vv (**Fig. 5B-C**), Vc (**Fig. 5B-C**), and in the Vd-r. Fiber density increases in the Vd-r from moderately dense in rostral sections to dense in more caudal regions (**Fig. 5B-C**). The postcommissural nucleus of the ventral telencephalon (Vp) and intermediate nucleus of the ventral telencephalon (Vi) contain moderately dense to dense fibers, and the lateral part of the supracommissural nucleus of the ventral telencephalon (Vs-l) has low density scattered fibers (**Fig. 5E-F**).

Diencephalon and mesencephalon

Overall, NPY-ir cells and fibers exist in great quantity throughout the diencephalon and mesencephalon of *A. burtoni* (**Fig. 5**). NPY-ir cells lie in the entopeduncular nucleus (E) (**Fig. 5E-F, 6D**), the parvocellular preoptic nucleus, anterior part (nPPa) (**Fig. 5E, 6E**), parvocellular preoptic nucleus, posterior part (nPPp), magnocellular preoptic nucleus parvocellular division (nPMp) (**Fig. 5E-F**), dorsal (NLTd), medial (NLTm), and ventral (NLTv) parts of the lateral tuberal nucleus (**Fig. 5G, 6F**), anterior tuberal nucleus (ATn) (**Fig. 5G, 6G**), and paraventricular organ (PVO) (**Fig. 5G**). Large cells (mean ± SD diameter; Gravid: 10.476 ± 2.001 μm; Brooding: 10.867 ± 1.471 μm) with distinct ventrally projecting fibers are also found in the dorsal tegmental nucleus (DT) (**Fig. 5I, 6H**). These cells are located in the same region as those identified as lying in the midbrain tegmentum of other fishes (Sakharkar et al., 2005; N. Subhedar, Cerda, & Wallace, 1996; Zahid, Malik, & Rani, 2014).

NPY-ir fibers lie in all preoptic nuclei including the nPPa, nPPp, magnocellular preoptic nucleus, parvocellular division (nPMp), magnocellular preoptic nucleus, gigantocellular division (nGMp), and nMMp (**Fig. 5D-F, 6E**). Low density fibers are primarily present in the rostral nPPa with a moderately dense population of fibers just ventral to the anterior commissure (ac) (**Fig. 5D**). Moderately dense to dense fibers are present in the area lateral to the rostral nPPa and ventral to the rostral E. Moderately dense fibers are also located in the nMMp, nPMp, nPPp, and nGMp (**Fig. 5F**).

In the rostral hypothalamus, NPY-ir fibers lie in the NLTd, NLTm, NLTv, lateral tuberal nucleus intermediate part (NLTi), ATn, lateral part of the diffuse nucleus of the inferior lobe (NDILI), nucleus of the lateral recess (NRL), nucleus of the posterior recess (NRP), and posterior tuberal nucleus (NPT) (**Fig. 5G-K**). Moderately dense varicose fibers are present in the ATn, which become denser towards the caudal ATn (**Fig. 5G**). The rostral NLTd has fibers with large varicosities, and the NLTv, NLTi, and NLTm have moderately dense fibers. In more caudal regions of these nuclei, the fibers are less dense (**Fig. 5G**). Low density fibers border the medial edge of the rostral NDILI , and in more caudal regions of NDILI, there are scattered, low density fibers positioned dorsally in the region ventral to the tertiary gustatory nucleus (TGN) (**Fig. 5G-J**). The rostral NRL has moderately dense fibers, while more caudal NRL regions have scattered fibers (**Fig. 5H-K**). The caudal part of the diffuse nucleus of the inferior lobe (NDILc) has low density fibers in the medial area dorsal to the NRL (**Fig. 5J-K**). Dense fibers are also present in the NRP (**Fig. 5H**) and in the NPT.

The rostral portion of the dorsal posterior thalamic nucleus (DP) contains dense fibers throughout, while the density is lower in more caudal sections (**Fig. 5G**). The

central posterior thalamic nucleus (CP) has moderately dense fibers in rostral sections, but fibers are less dense and confined to the center of the nucleus in more caudal regions (**Fig. 5G**). Moderately dense fibers are seen in the ventral habenular nucleus (nHv) and more scattered fibers in the dorsal habenular nucleus (nHd). Low to moderately dense fibers exist in most nuclei of this region, including PVO, periventricular nucleus of the posterior tuberculum (TPp), ventromedial thalamic nucleus (VMn), periventricular pretectal nuclei (PPv, PPd), anterior thalamic nucleus (An), nucleus pretectalis (NP), superficial pretectal nucleus intermediate division (PSi), lateral preglomerular nucleus (PGl), TGN, and nucleus of the torus lateralis (TLa), as well as regions adjacent to these nuclei (**Fig. 5G**). Dense fibers are present in the central pretectal nucleus (NPC), central thalamic nucleus (CTn), and nucleus corticalis (NC). Fibers are primarily absent from the large PGn and corpus mammillare (CM) nuclei along the midline (**Fig. 5H-I**), although there are an occasional few scattered varicose fibers in some sections.

Moderately dense NPY-ir fibers lie consistently in the tectum (T), primarily in the region between the periventricular gray zone (PGZ) and deep white zone of tectum (DWZ), but were also scattered throughout the central zone (CZ) and superficial gray and white zone (SWGZ) (**Fig. 5F-K**). Low density fibers are found in the lateral tegmental nucleus (LT), DT, nucleus of the medial longitudinal fasciculus (nMLF), oculomotor nucleus (IIIn), and glomerular nucleus (Gn) (**Fig. 5H-J**). Low to moderately dense fibers are also found in the torus semicircularis (TS), specifically the central nucleus of TS (TSc), with scattered fibers in the ventrolateral nucleus (TSvl) (**Fig. 5H-**

K). Moderately dense fibers lie in the central part of the nucleus of the lateral valvulae (NLVc) and paratoral tegmental nucleus (PTT) (**Fig. 5I-J**).

Rhombencephalon

NPY-ir cells lie in the central gray (CG) surrounding the fourth ventricle (**Fig. 5K**), and in the inferior olive (**Fig. 5M**). In general, NPY-ir fibers are scarcer in the rhombencephalon compared to the telencephalon, diencephalon and mesencephalon. Scattered fibers are present in the Purkinje cell layer of the corpus cerebelli (CCeP) and valvula cerebelli (VCeP) (**Fig. 5K-L**). Low to moderately dense fibers exist in the secondary gustatory nucleus (SGn), and the region lateral to the isthmal nucleus (NI) (**Fig. 5K**). Low density fibers are found throughout the rostro-caudal CG (**Fig. 5J-K**), as well as scattered fibers in NI, medial longitudinal fasciculus (mlf) (**Fig. 5J-L**), Raphe nucleus (SR), interpeduncular nucleus (IP), and within several octavolateralis nuclei (**Fig. 5K-L**). Dense fibers lie in the region between the medial reticular nucleus and secondary gustatory tract (sgt) (**Fig. 5L**). Low density fibers are also present in the inferior (Ri), medial (Rm), and superior (Rs) nuclei of the reticular formation (**Fig. 5J-L**). Moderately dense to dense fibers are found bordering the dorsal portion of the vagal lobe (VL) and moderately dense fibers are present within the VL (**Fig. 5M**). Low to moderately dense fibers lie in the medial funicular nucleus (MFN) and descending trigeminal tract (dtt) (**Fig. 5N**).

Localization of *npy* neurons - ISH

In the olfactory bulbs, *npy* cells are abundant in the ICL, which was not observed with antibody staining (**Fig. 7A**). In the telencephalon, some scattered cells are found

along the midline in Dm-1 and in the rostral Dl-d and Dc, while cells are numerous in the subpallial Vv, dorsal part of the ventral telencephalon (Vd), Vc, Vl, Vi, Vp, and supracommissural nucleus of the ventral telencephalon (Vs) (**Fig. 7B,C**). Cells within some of these ventral telencephalic regions (notably the Vs), however, did not appear stained with immunohistochemistry. *npy* cells are also found in the entopeduncular nucleus, nPPa, nPPp, and nMMp, and in the region ventral to the habenula (possibly in the nucleus of the thalamic enimentia, nTE) (**Fig. 7D**). Similar to IHC, cells are also expressed in the ATn, PVO, and NLT (**Fig. 7E**). In the mesencephalon, *npy* cells are abundant in the PGZ of the tectum (**Fig. 7E**), and some scattered cells in the torus semicircularis (primarily TSc). No cells were observed in any cerebellar nuclei (valvula or corpus cerebelli). In the rhombencephalon, cells lie in the SGn and secondary visceral nucleus (SVn), and scattered cells are found in the CG below the fourth ventricle, in the inferior olive nucleus (IO), in reticular formation nuclei, and in the MFN of the rostral spinal cord above the central canal (**Fig. 7F-H**). Overall, there are many more cells stained with ISH compared to IHC, including some that were not labeled at all with IHC (e.g. PGZ, IO, SGn, SVn, Vs, ICL, etc.) and some that stained intensely with IHC but were only weakly stained with ISH (e.g. gTN, DT).

Localization of AGRP-immunoreactivity

Olfactory bulbs and telencephalon

There are no AGRP-ir cells in the olfactory bulbs. A few scattered -ir fibers lie in the ventro-medial area of the ECL and in the medial area of the ICL (**Fig. 8A**).

There are also no AGRP-ir cells found anywhere in the telencephalon, but AGRP-ir fibers lie in both dorsal and ventral telencephalon regions (**Fig. 8A-D**). In the dorsal telencephalon, low density scattered fibers are present in the rostral portion of Dm-1, Dc-1, Dl-d, and Dl-v2 (**Fig. 8A-C**). Fibers are primarily absent from the medial part of the dorsal telencephalon (Dm), with the exception of scattered fibers in rostral Dm-1 (**Fig. 8A**). In the ventral telencephalon, moderately dense AGRP-ir fibers lie in the rostral Vs-m, and scattered moderately dense fibers in the Vd-r and the caudal subdivision of Vd (Vd-c) (**Fig. 8B-C**). Dense to moderately dense fibers are found throughout Vv (**Fig. 9A**), as well as scattered fibers in the region lateral to the caudal portion of Vv and within Vp (**Fig. 8B-D**).

Diencephalon and mesencephalon

AGRP-ir cells lie in the NLT; the rostral portion of the NLTv contains cells along the lateral edge that are then located in a more medial position in the caudal portion of this nucleus (**Fig. 8F, 9D**).

In the preoptic nuclei, AGRP-ir fibers are abundant in the nPPa, nMMp, nPMp, nPPp, and nGMp (**Fig. 8D-E, 9B**). Dense fibers are present in the nPPa and nPMp, while moderately dense fibers are present in the nPPp (**Fig. 8D-E**). The rostral nMMp contains moderately dense fibers, which increase in density towards the caudal nMMp (**Fig. 8D**). The regions lateral to these preoptic nuclei also contain moderately dense fibers (**Fig. 8D**).

In the hypothalamus, low density AGRP-ir fibers lie in NLTd, NLTi, NLTm, and NLTv (**Fig. 8E-F, 9C-D**). Low to moderately dense fibers also lie in ATn (**Fig. 8F, 9F**), and scattered fibers are present in some more caudal diencephalic regions such as the

medial nucleus of the interior lobe (NMIL) bordering the ventral side of the glomerular nucleus (Gn), and in NDILl (**Fig. 8G-H**). Fibers are scattered in the NRL and are present throughout the entire rostro-caudal extent of this nucleus (**Fig. 8G-J, 9E**).

In the thalamic region, scattered fibers exist in DP, CP, and VMn, as well as in ventral (nHv) and dorsal (nHd) nuclei of the habenula (**Fig. 8E-F**). Scattered, low density fibers are also present in the posterior tuberal nucleus (PTN) and TPp (**Fig. 8F**). The tectum consistently contains scattered AGRP-ir fibers located in the CZ, PGZ, DWZ, and SWGZ (**Fig. 8E-H**). Scattered, low density fibers are present in the medial portion of llln (**Fig. 8H**). Scattered fibers also exist in the rostral PTT, the torus semicircularis (TSc and TSvl), and in regions surrounding Gn and the medial preglomerular nucleus (PGm) (**Fig. 8G-H**).

Rhombencephalon

No AGRP-ir fibers are seen in the corpus or valvula cerebelli. Scattered low density AGRP-ir fibers lie in the rostral CG around the fourth ventricle. In more caudal regions of CG, there is an increase in fiber density (**Fig. 8J**), but it is again low in the most caudal portion of the CG (**Fig. 8K**). Moderately dense fibers are present in the area between the CG and Rs, and scattered fibers lie within reticular nuclei (Rs, Rm, Ri) (**Fig. 8J-L**), SGn, SR, facial lobe, vagal lobe (VL), and the MFN of the rostral spinal cord (**Fig. 8J-M**).

Localization of *agrp* neurons – ISH

In situ hybridization labels *agrp* neurons solely within the hypothalamic NLTv, which is consistent with the somata labeling observed with immunohistochemistry (**Fig. 2A-B**).

Localization of CART-immunoreactivity

Olfactory bulbs and telencephalon

There are no CART-ir cells in the olfactory bulbs. CART-ir fibers lie primarily in the ICL, but there are also some scattered fibers in the ECL and lateral margin of the rostral GL (**Fig. 8A**).

In the telencephalon, CART-ir cells lie in the rostral Vv (**Fig. 8B-C, 10C**), in Vl (**Fig. 8B**), and in the lateral part of Vc (**Fig. 8B-C, 10A**). CART-ir fibers are found to some extent in all parts of the dorsal telencephalic nuclei (**Fig. 8A-D**). Low density CART-ir fibers lie in Dl-v1, Dl-v2, and dorsal portion of Dl-d (**Fig. 8A-C**), while scattered fibers are present in all Dm regions (**Fig. 8A-D**), throughout Dd, and in the posterior part of the dorsal telencephalon (Dp) (**Fig. 8D**). CART-ir fibers also lie in all Dc regions, with moderate fiber densities in some rostral regions of Dc-1 and the lateral region of Dc-2, and more scattered distributions in caudal Dc-1, and in Dc-3, Dc-4 and Dc-5 (**Fig. 8A-D**).

CART-ir fibers are also present to some extent in all parts of the ventral telencephalic nuclei (**Fig. 8B-D**). Fibers exist in low density in the rostral Vd-r, with a transition to moderate density in more caudal regions (**Fig. 8B-C**). Low density scattered fibers are also present in Vv, Vl, Vc, and Vp (**Fig. 8B-D**). In the Vs-m, low density fibers are found in rostral sections bordering the dorsal portion of Vd-c, and then

become scattered throughout the caudal extent of Vs-m (**Fig. 8C-D**). In the Vd-c, low density fibers lie in the dorsal region bordering the ventral portion of Vs-m (**Fig. 8C**).

Diencephalon and mesencephalon

CART-ir cells lie in the entopeduncular nucleus (E) (**Fig. 8D, 10B**), medial area of the ventral nPPp (**Fig. 8E, 10D**), NLTv (**Fig. 8F, 10E**), and NRP (**Fig. 8G, 10G**). A small group of CART-ir cells also lies in the thalamus just lateral to DP and CP (**Fig. 8F, 10F**). Large CART-ir cells (mean ± SD diameter: Gravid: 9.543 ± 1.146 μm; Brooding: 9.663 ± 1.180 μm) are also found in the medial region of the nMLF situated dorsal to the mlf, and in DT (**Fig. 8G-H, 10H**).

Moderately dense CART-ir fibers are present in the preoptic nuclei of the diencephalon, including nPPa, nPMp, nMMp, nGMp, and nPPp (**Fig. 8D-E**). In the hypothalamus, fibers are present in NLTv, NLTd, NLTi, NDILl, NRL, and medial part of the diffuse nucleus of the inferior lobe (NDILm) (**Fig. 8F-I**). The NLTv, NLTi and ATn have low to moderately dense fibers scattered throughout their rostro-caudal extents, while the rostral NLTd has only a few scattered fibers (**Fig. 8F**). The NRL has low to moderately dense fibers located around the lateral recess with fibers primarily on the medial side in the region just dorsal to the NDILm (**Fig. 8I**). The NDILl has a few scattered fibers throughout the nucleus while more dense fibers are found dorsally between the NDILl and the Gn and NMIL (**Fig. 8I**).

CART-ir fibers are found to some extent throughout all thalamic and pretectal nuclei (**Fig. 8E-F**). In the thalamus, DP, CP, and VMn contain scattered low density CART-ir fibers (**Fig. 8E-F**). The PPd and PPv have scattered low density fibers confined to the dorsal portion of the nucleus that borders the posterior commissure (pc). The nTE

has low density fibers confined to the medial portion of the nucleus. The TPp has a few scattered fibers throughout its rostro-caudal extent (**Fig. 8F**), and low density fibers are found bordering the ventral area around the Gn (**Fig. 8H**).

In the tectum, fibers lie consistently throughout the SWGZ, DWZ, CZ, and PGZ (**Fig. 8D-K**). The SWGZ has scattered fibers while there are more numerous fibers in CZ, and dense fibers between the DWZ and PGZ (**Fig. 8E-K**). CART-ir fibers are dense along the midline in the mesencephalon, with regions such as PGn, CM, and Gn either devoid of fibers or containing only a few scattered fibers (**Fig. 8G-H**). The regions surrounding these nuclei, however, contain moderate to high density fibers. The llln, nMLF, LT, and DT contain some scattered fibers (**Fig. 8H-I**). The torus longitudinalis (TL) also has a few scattered fibers throughout its rostro-caudal extent (**Fig. 8G-H**). CART-ir fibers are abundant in the TS, with moderate to dense fibers in TSc, particularly along the dorsal margin, and moderate to low density fibers in TSvl (**Fig. 8G-J**). The PTT and NLVc also contain scattered CART-ir fibers (**Fig. 8H-I**).

Rhombencephalon

Overall, CART-ir fibers are scattered and less numerous in the rhombencephalon compared to more rostral brain areas (**Fig. 8J-M**). Some scattered fibers lie in the granular (VCeG) and molecular (VCeM) layers of valvula cerebelli, with slightly greater densities found in VCeP (**Fig. 8G-I**). Similarly, low density fibers lie in CCeP, with some occasional scattered fibers in the granular (CCeG) and molecular (CCeM) layers of corpus cerebelli (**Fig. 8J-K**). CART-ir fibers are scattered in SGn, but only an occasional sparse fiber is seen in NI (**Fig. 8J**). The rostral CG has a few scattered fibers bordering the fourth ventricle and moderately dense to dense fibers in the caudal CG (**Fig. 8K-L**).

Rs and Rm have low density scattered fibers throughout, and a few fibers are seen within the mlf (**Fig. 8J-L**). Low density CART-ir fibers are scattered in SR along the midline (**Fig. 8J**), in all octavolateralis nuclei of the hindbrain, in the facial lobe, and along the ventro-lateral regions of the hindbrain (**Fig. 8J-L**). Low density fibers are also found throughout the VL (**Fig. 8L**), while low to moderately dense fibers lie in the MFN and dtt of the rostral spinal cord (**Fig. 8M**).

Localization of *cart2* and *cart4* – ISH

The distribution of *cart4* cells in the brain is more restricted than the widespread staining of *cart2* neurons (**Fig. 11**). No *cart4* cells are detected in the telencephalon, and notably, *cart4* cells are absent from NLT. *cart4* cells lie in the habenula (nHd), VMn, intercalated nucleus (IC), and TPp (**Fig. 11A-C**). A distinct cluster of large *cart4* cells lies in DT (**Fig. 11D**), and in the rhombencephalon, cells are found in CG, Ri, and scattered within the sensory VL (**Fig. 11E-F**). The only *cart4* cells labeled with the CART antibody are those in DT.

In contrast to *cart4*, *cart2* cells are abundant and widely distributed throughout the entire brain (**Fig. 12**). Numerous cells lie in the ICL of the olfactory bulbs (**Fig. 12A**), and some scattered cells are seen in rostral Dm, Dd, and lateral parts of the dorsal telencephalon (Dl). Numerous *cart2* cells also lie within several Dc nuclei (Dc-3, -4, -5), along with more sparse cells in Dc-1 (**Fig. 12B-D**). *cart2* cells are abundant in Vv, Vc, Vl, and Vi of the subpallium (**Fig. 12B-C**). In the preoptic nuclei, *cart2* cells localize primarily to nPPa, nPPp, and nMMp (**Fig. 12C,E**). Moving caudally, *cart2* cells lie in many diencephalic and mesencephalic regions including the parvocellular superficial

pretectal nucleus (PSP), PPd, PPv, prethalamic nucleus (PN), PGm, PGl, DP, TPp, PVO, ATn, NLT, posterior thalamic nucleus (PT), TLa, nMLF, NPT, NRP, CM, NMIL, and NRL (**Fig. 12F-I**). Cells also surround PGn and Gn, and are present in LT, TS (primarily TSc), and PGZ of the tectum (**Fig. 12G,I,J**). In the rhombencephalon, distinct *cart2* cells lie in CG, SGn, SVn, LC, SR, IO, and reticular formation nuclei (**Fig. 12J**). *cart2* cells are also scattered in the sensory VL, throughout most hindbrain octavolateralis nuclei, and in the MFN of the rostral spinal cord (**Fig. 12K-L**). No cells exist in any cerebellar nuclei (valvula or corpus cerebelli). The *cart2* neurons that are also labeled with CART immunohistochemistry include Dm-1, Vc/Vl, nPPp, nMLF, and NRP.

Reproductive state differences in somata size

NPY-ir (mean ± SE; Gravid: 19.792 ± 0.869 μm^2; mouth brooding: 13.057 ± 0.918 μm^2) and AGRP-ir (Gravid: 16.035 ± 0.636 μm^2; mouth brooding: 11.672 ± 0.636 μm^2) mean somata sizes in the NLT are larger in gravid females compared to brooding females (NPY: ANCOVA; F=24.531; df=18; $P<0.001$; AGRP: ANCOVA; F=20.529; df=19; $P<0.001$) (**Fig. 13A-B**). *Pomc1a* mean somata sizes are larger in brooding compared to gravid females (ANCOVA; F=19.401; df=17; $P<0.001$) (Gravid: 22.898 ± 1.197 μm^2; mouth brooding: 30.702 ± 1.197 μm^2) in the NLT (**Fig. 13C**). Correlations between somata sizes, GSI, and HSI for gravid and brooding females combined are summarized in **Table 3**. There is a negative correlation between *pomc1a* somata size and GSI. *Pomc1a* somata size is also negatively correlated with both NPY-ir and AGRP-ir somata sizes. NPY-ir and AGRP-ir somata sizes both show a positive

correlation with GSI. HSI is not correlated with any of the neuropeptide somata sizes. However, there were no significant correlations among any variables when gravid females (all R<0.60; *P*>0.05) and brooding females (all R<0.40; *P*>0.05) were run separately.

Hypothalamic mRNA expression differences between gravid and brooding females

A total of 28 (15 gravid, 13 brooding) females were used in the hypothalamic mRNA analysis. Similar to the females used for neuropeptide-containing somata quantification analyses described above, gravid females have higher GSI (mean±SD; 10.08 ±1.35) (Mann-Whitney; U=0.00; *P*<0.001) and larger ova diameters (2.35 ± 0.30 mm) (Mann-Whitney; U=0.00; *P*<0.001) compared to brooding females (0.71±0.23 mm). Gravid females also have higher HSI (1.66 ± 0.61) values compared to brooding females (0.86 ± 0.33) (Mann-Whitney; U=19.00; *P*<0.001), and higher condition factors compared to brooding females (gravid: 3.90 ± 0.41; mouth brooding: 3.06 ± 0.43) (Student's t-test; *P*<0.001; t=5.346; df=26), indicative of greater energy reserves and overall fitness. Standard length (Student's t-test; *P*=0.152; t=-1.475; df=26) and body mass (Student's t-test; *P*=0.0796; t=1.824; df= 26) did not differ between gravid and brooding females. Macro-dissected hypothalamic mRNA levels for *agrp, cart2, cart4, ghrelin receptor (ghs-r1), leptin receptor (lepr), npy, and pomc1a* were compared between gravid and brooding females. *Agrp* mRNA expression is significantly higher in gravid females compared to brooding females, but there are no differences between gravid and brooding females for any of the other mRNA levels measured (**Table 4**).

Correlations between hypothalamic mRNA levels for all fish combined are summarized in **Table 5**. *Pomc1a* mRNA levels positively correlate with *agrp* mRNA levels in the hypothalamus, and *npy* mRNA levels positively correlate with mRNA levels of the receptors, *ghs-r1 and lepr.* When gravid and brooding animals were analyzed separately, only a single positive correlation between *lepr* and *agrp* was evident in brooding females (R=0.75, P=0.021). In contrast, gravid females showed many positive correlations between candidate gene mRNA levels in the hypothalamus: *pomc1a* with *agrp* (R=0.74, P=0.003), *cart2* (R= 0.55, P=0.04), and *npy* (R=0.68; P=0.007); *agrp* with *ghs-r1* (R=0.61, P=0.02), *cart2* (R=0.75, P=0.002), *lepr* (R=0.61, P=0.015), and *npy* (R=0.80, P<0.001); *ghs-r1* with *lepr* (R=0.59, P=0.03); *cart2* with *lepr* (R=0.72, P=0.003) and *npy* (R=0.83, P<0.001); and *lepr* with *npy* (R=0.85, P<0.001).

DISCUSSION

Our results provide the first localization maps of NPY, AGRP, and CART neurons throughout the entire brain of a mouth brooding teleost fish. We demonstrate that these neuropeptides are found in brain regions that regulate feeding, energy status, and reproduction that are conserved with those of higher vertebrates. Future studies should conduct co-labeling experiments to test whether any of these neuropeptides are expressed in the same or different neurons, particularly in the NLT. Further, we show that somata size of *pomc1a*, AGRP, and NPY-producing neurons differs between gravid and mouth brooding *A. burtoni* females, suggesting that changes in the synthesis, release, or neural activity of these neurons is important for regulating cyclical variations between these different energetic and reproductive states.

Comparisons of NPY, AGRP, and CART with other teleosts

Neuropeptide Y (NPY)

Moderate NPY-immunoreactive fibers were detected in all layers of the olfactory bulb (ECL, ICL, GL, SOF) in *A. burtoni*, which is similar to other fish species including tilapia (Sakharkar et al., 2005), goldfish (Pontet et al., 1989), and the ayu (Chiba, Oka, & Honma, 1996). NPY-ir cells were not detected in the olfactory bulbs of *A. burtoni,* which is similar to the Senegalese Sole (Rodriguez-Gomez, Rendon-Unceta, Sarasquete, & Munoz-Cueto, 2001), but differs from other species such as the goldfish (Pontet et al., 1989), senegal bichir (Reiner & Northcutt, 1992), and ayu (Chiba et al., 1996), in which NPY-ir cells were present in the ECL of the olfactory bulbs. However, *npy* mRNA was abundant in cells of the ICL in the olfactory bulbs in *A. burtoni*, which is consistent with that seen in the sea bass *Dicentrarchus labrax* (Cerda-Reverter et al., 2000). The presence of NPY-ir fibers and *npy* cells in the olfactory system suggests a modulatory role in olfactory processing, possibly related to appetite and hunger level of the animal, similar to that described in the axolotl (Mousley, Polese, Marks, & Eisthen, 2006).

In the telencephalon of *A. burtoni*, NPY-immunoreactive cells were found in the Vd-r, Vl, Vc, and Dc, and –ir fibers were present throughout the dorsal and ventral telencephalon. This NPY-ir fiber pattern is generally similar to that reported in other teleosts (Batten, Cambre, Moons, & Vandesande, 1990; Chiba et al., 1996; Danger et al., 1991; Gaikwad et al., 2004; Kah et al., 1989; Pontet et al., 1989; Sakharkar et al., 2005; N. Subhedar et al., 1996). NPY-immunoreactivity in *A. burtoni* was also present in

various regions that are homologous to mammalian nuclei involved in feeding and reproduction. For example, NPY-ir cells were present in the entopeduncular nucleus (E), which is consistent with findings in goldfish (Pickavance, Staines, & Fryer, 1992), rainbow trout (Danger et al., 1991), catfish (Gaikwad et al., 2004), killifish (N. Subhedar et al., 1996), and carp (Marchetti et al., 2000). While the definitive homolog of the entopeduncular region is not known in teleosts, the mammalian entopeduncular region is part of the amygdala (O'Connell & Hofmann, 2011). However, the entopeduncular nucleus is also thought to play a role in reproduction. In castrated male tilapia, for example, depletion of NPY immunoreactivity in E neurons was evident post-castration, but was restored following testosterone treatments (Sakharkar et al., 2005), suggesting a reproductive role for the NPY-ir cells in E. The prevalent NPY-immunoreactivity in the telencephalon of teleosts suggests widespread modulatory roles in reproduction, sensory processing, decision-making, and social and other life-history behaviors. For example, in the preoptic area of *A. burtoni,* NPY-ir cells were present in nPPa, nMMp, and nPMp, and fibers were found throughout all preoptic nuclei. In teleosts, the importance of the preoptic area in reproduction is well established because it contains GnRH1 neurons that project directly to the pituitary to stimulate the synthesis and release of gonadotropin hormones. In *A. burtoni*, NPY-ir cells were also present in the NLT, the teleost homolog to the mammalian arcuate nucleus (Cerda-Reverter & Peter, 2003; Liu et al., 2010) involved in the control of energy balance and feeding behavior. Thus, the present study suggests that NPY's role in regulating feeding and reproductive functions is likely conserved.

Agouti-Related Protein (AGRP)

AGRP-immunoreactivity in the olfactory bulb of *A. burtoni* was restricted to a few fibers in the ICL. This is similar to zebrafish where fibers were found in the olfactory bulbs, however, they were not restricted to a particular cell layer (Forlano & Cone, 2007). Therefore, the presence of AGRP in the olfactory bulbs of *A. burtoni* suggests a conserved neuroanatomical distribution, but examinations in more species are needed. The presence of AGRP in the olfactory bulb could suggest a role in olfactory processing, specifically in conjunction with the melanocortin system. α-MSH-ir fibers are present in the olfactory bulbs of zebrafish and the MC4 receptor was present in the olfactory bulb of the spiny dogfish (Ringholm et al., 2003), suggesting that AGRP may modulate olfactory processing related to feeding and energetic status.

AGRP-ir cells in *A. burtoni* are found exclusively in the NLT of the hypothalamus. This is consistent with findings in goldfish (Cerda-Reverter & Peter, 2003), zebrafish (Forlano & Cone, 2007), and sea bass (Agulleiro et al., 2014), where AGRP is mainly expressed in the caudal portion of the NLT. This region of the brain is associated with feeding and energy expenditure in teleosts (Forlano & Cone, 2007), and is considered the homolog of the arcuate nucleus in mammals because it expresses the specific arcuate markers, AGRP and POMC. In some fishes, fasting up-regulates brain mRNA levels of *agrp* [e.g. goldfish (Cerda-Reverter & Peter, 2003) and zebrafish (Song et al., 2003)], while in other species fasting decreases *agrp* levels [e.g. common carp (Wan et al., 2012)]. Nevertheless, most studies suggest that AGRP also functions as a feeding modulator in teleost fishes. AGRP and NPY are co-expressed in the same neurons in mammals, but further double label studies are necessary to determine if this is also true

in *A. burtoni* and other teleosts. Our study provides further evidence that the neuroanatomical distribution of AGRP is conserved and suggests that the mechanisms regulating energy homeostasis may be similar across vertebrates.

Cocaine and amphetamine-regulated transcript (CART)

CART-immunoreactivity was absent from the SOF and gTN of *A. burtoni,* but CART-immunoreactive fibers were observed in the ICL, ECL and GL of the olfactory bulb, which is consistent with previous findings in catfish (Singru et al., 2007) and zebrafish (Akash et al., 2014), suggesting a role for CART in the processing of olfactory information in teleosts. Similarly, in rats, low density CART-ir fibers were found in the inner plexiform layer, and CART-ir cells were present in the mitral and outer plexiform layers of the olfactory bulbs (Couceyro, Koylu, & Kuhar, 1997; Koylu, Couceyro, Lambert, & Kuhar, 1998). Further, CART peptide was found in the mitral cells of the rat olfactory bulb , suggesting a role for CART in the processing of olfactory signals in mammals as well (Couceyro et al., 1997; Koylu et al., 1998). In *A. burtoni*, *cart2* cells were also abundant in the ICL, which is consistent with that in the zebrafish (Akash et al., 2014). Taken together, these findings suggest a role for CART in the processing of olfactory information in vertebrates that warrants further investigation with a comparative approach. Further, the wide distribution of CART-ir fibers in brain regions that process other sensory information (e.g. visual, auditory, mechanosensory) in *A. burtoni* and other fishes (Mukherjee et al., 2012) suggests additional functions in sensory integration.

CART-immunoreactivity was also present in neuroendocrine regulatory areas of

the telencephalon and diencephalon in *A. burtoni*. For example, CART-ir cells were present in the entopeduncular nucleus, which is congruent with studies done in the catfish (Mukherjee et al., 2012; Singru et al., 2007) and zebrafish (Akash et al., 2014). In contrast, however, CART-immunoreactivity was not observed in the entopeduncular nucleus of the frog *Rana esculenta* (Lazar, Calle, Roubos, & Kozicz, 2004). This suggests that there may be species or taxa-specific differences across vertebrates. CART-ir somata were also present in the nPPp of *A. burtoni*, and fibers were present throughout the preoptic nuclei, which is consistent with other teleosts. Further, *cart2* cells were detected in several preoptic nuclei via *in situ* hybridization in *A. burtoni*. In zebrafish, *in situ* hybridization experiments showed *cart2* and *cart4* cells in nPPa and nPPp (Akash et al., 2014), and immunostaining experiments demonstrated a dense CART-ir fiber network in the preoptic area (Mukherjee et al., 2012). In catfish, dense immunoreactivity was also seen in the preoptic area, which also varied seasonally and with reproductive state (Barsagade et al., 2010). The preoptic area of teleosts is well-recognized as an important node in the regulation of reproduction (Yu, Rosenblum, & Peter, 1991) and contains neurons that innervate the pituitary gland (e.g. GnRH1 cells), which regulate hypophysiotropic functions such as gonadotropin hormone secretion (Akash et al., 2014; Zohar, Munoz-Cueto, Elizur, & Kah, 2010). In mammals, CART-immunoreactive fibers were observed in close proximity to GnRH cells in the preoptic area [Siberian hamster; (Leslie et al., 2001), and pig; (Bogus-Nowakowska et al., 2011)], and the CART-expressing neurons in the arcuate nucleus and premammilary ventral nucleus communicate with GnRH containing neurons in the POA. It is thought that this circuitry modulates GnRH1 secretion resulting in a surge of luteinizing

hormone, as well as facilitating leptin's effect on GnRH secretion (Rondini, Baddini, Sousa, Bittencourt, & Elias, 2004; N. K. Subhedar, Nakhate, Upadhya, & Kokare, 2014). A recent study by True et al. (2013) showed that CART had extensive connectivity with GnRH1 and kisspeptin-expressing neurons in the preoptic area, and electrophysiology experiments showed that CART post-synaptically depolarized both GnRH1 and kisspeptin cells (True, Verma, Grove, & Smith, 2013). In addition, CART mRNA expression and the number of CART-immunoreactive cells decreased during calorie restriction, suggesting that CART expression in animals of depressed metabolic conditions could inhibit the reproductive axis (N. K. Subhedar et al., 2014; True et al., 2013). Overall, this conserved neuroanatomical distribution from fishes to mammals suggests a potential mechanism by which nutritional status is conveyed to the reproductive system via circuitry that involves the preoptic nuclei of vertebrates.

CART-immunoreactivity is also observed in regions associated with the regulation of feeding, energy balance, and gustation in teleosts. These areas include the E, NLT, NRL, and NDIL, which all showed CART immunoreactivity in *A. burtoni*. This is consistent with previous findings that demonstrated CART-ir somata in the NLT of zebrafish and catfish (Akash et al., 2014; N. K. Subhedar et al., 2014). In zebrafish, starvation led to a reduction in *cart2*-expressing neurons of the E and NRL, and *cart4*-expressing neurons in the NLT (Akash et al., 2014). Thus, CART may have a central role in the regulation of energy balance and feeding in teleosts, similar to that described in mammals (Lin et al., 2000; N. K. Subhedar et al., 2014; Volkoff et al., 2005). Due to the whole genome duplication event in teleosts, multiple *cart* genes are reported in zebrafish (Akash et al., 2014) and in *A. burtoni* (Hu et al., 2016), and our ISH results

showing divergent distributions for *cart2* and *cart4* suggest subfunctionalization. Further studies are needed to examine functional differences of these different forms.

Reproductive state differences in somata size and mRNA expression

Neurons are responsible for the coordination and regulation of gene expression in response to functional needs of the organism (Ransdell, Faust, & Schulz, 2010); however, there are not always straightforward relationships between somata size, cell number, mRNA levels, and protein levels within individual neuron types. For example, a study in the European starling (*Sturnus vulgaris*) showed that changes in the number of GnRH1 and gonadotropin-inhibitory hormone (GnIH) cells throughout the breeding season, overall, mirror changes in neuronal somata size and estimated peptide concentration (Calisi, Diaz-Munoz, Wingfield, & Bentley, 2011). That study, therefore, showed a positive relationship between cell number, cell size, and peptide concentration. In another study done in Japanese quail and domestic chickens, the authors double-labeled for NPY using IHC and ISH and demonstrated the coexistence of *npy* mRNA and NPY peptide in individual cells (Boswell, Millam, Li, & Dunn, 1998). This suggests that these cells are both transcribing *npy* mRNA as well as storing the peptide. Therefore, an increase in cell size could be due to an increase in peptide production *or* reduced peptide release and storage, but it is not possible to distinguish amongst these possibilities via staining techniques alone.

In our study, we tested whether neuron somata size and gene expression for candidate orexigenic and anorexigenic genes varied based on reproductive and energy consumption states. Our results showed larger NPY-ir and AGRP-ir somata in gravid

compared to brooding females, and larger *pomc1a* somata in brooding compared to gravid females. One explanation for the changes in cell size between gravid and brooding females could be the need for mechanisms that allow quick adaptive changes in the neuroendocrine system without cell addition or cell death (Francis, Soma, & Fernald, 1993). For example, somata that increase in volume can support more complex dendritic inputs, which can have important functional implications for the response properties of individual neurons within the circuit (Mainen & Sejnowski, 1996; Roberts, Best, & Suter, 2006). This is potentially important in mouth brooding fish such as *A. burtoni,* as females undergo a fairly rapid transition from a gravid (energy investment) to a brooding (energy consumptive) state when her clutch of eggs is effectively transferred from her abdominal cavity into her buccal cavity during spawning. During this "motivational switch" from a self-promoting to an offspring-promoting phenotype, it is important that the neurons involved in regulating the accompanying behaviors and physiology demonstrate plasticity, especially when food intake is no longer physically possible. There is also a precedent for rapid changes in somata size in male *A. burtoni*, since GnRH1 neurons enlarge within the first 24 hrs of a transition from reproductively-suppressed subordinate to reproductively-active dominant social status (Maruska, 2014; Maruska & Fernald, 2013). Thus, rapid changes in cell size may be a common mechanism mediating phenotypic plasticity within different neuroendocrine systems for both males and females of this species.

To further investigate the involvement of these candidate neuropeptides in the regulation of the neural control of the mouth brooding parental care strategy, including the period of necessary food-deprivation, RT-qPCR was performed on macro-dissected

hypothalamic tissue. We demonstrate that levels of hypothalamic *agrp* were higher in gravid compared to brooding females, which mirrors the observed differences in AGRP-ir somata sizes. The difference between reproductive states could be explained by AGRP's role as a melanocortin antagonist, and therefore, higher *agrp* mRNA levels in gravid females may contribute to regulation of the melanocortin system by inhibiting the binding of α-MSH to the MC4 receptor, maintaining high food intake during the consumptive gravid phase. This is important because the females need to build up metabolic stores in addition to undergoing vitellogensis, which would ensure that the female carries to term and does not pre-release or cannibalize her fry. In mammals, AGRP inhibition of POMC neurons is thought to be more important for long-term regulation of appetite than the short-term feeding behaviors typically stimulated by AGRP neuron activation (Sternson & Atasoy, 2014). Thus, AGRP neurons show bidirectional control of feeding behavior, and increased mRNA levels in gravid female *A. burtoni* may reflect changes in the maintenance of feeding during their energy investment period.

In the current study, hypothalamic mRNA levels of all other candidate genes did not differ between gravid and brooding female *A. burtoni*, and we offer several potential explanations below. First, while the females are brooding, they are physically incapable of eating so our initial prediction was that *lepr* mRNA expression would be higher during this reproductive stage, thereby increasing the sensitivity of the hypothalamus to the leptin signal to prevent the females from cannibalizing or releasing their brood. On the other hand, gravid females have to maintain their caloric intake while they undergo vitellogenesis and ovarian recrudescence, so our initial prediction was that they would

have higher levels of *ghs-r1* mRNA to maintain feeding motivation and food intake. In the current study, however, mRNA levels of ghrelin receptors and leptin receptors did not differ between gravid and brooding females, so it is possible that fasting/feeding does not influence transcription, but may modify the density or turnover of receptors in certain neurons, or occur on shorter time scales (Cerda-Reverter et al., 2011). During fasting, for instance, the availability of receptors could be reduced, thereby decreasing sensitivity to hormones such as ghrelin, orexigenic neuropeptides such as NPY and AGRP, or constitutive signaling of hormones and neuropeptides.

Second, there were also no differences in hypothalamic mRNA expression of *pomc1a* and *npy* between gravid and brooding *A. burtoni* females. These results are similar to other studies that demonstrated little to no change in *pomc* hypothalamic mRNA levels associated with variations in feeding and fasting state in fishes (Cerda-Reverter et al., 2011; Sanchez, Rubio, & Cerda-Reverter, 2009). Thus, regulation of *pomc* neurons during prolonged fasting may involve other mechanisms such as differential processing of *pomc* precursors or changes in melanocortin receptor expression rather than changes in mRNA levels. Similar to our results for *npy*, a previous study in *A. burtoni* also found no differences in whole brain *npy* expression among gravid (fed), starved, and brooding (starved) females (Grone et al., 2012). Studies in other fishes show considerable variation in the response of *npy* mRNA levels to feeding conditions (Murashita, Kurokawa, Ebbesson, Stefansson, & Ronnestad, 2009; Yan et al., 2017; Yokobori et al., 2012). Thus, the regulation of *npy* mRNA may vary between species that differ in diet, digestive physiology, and metabolic trade-offs associated with life-history characteristics such as parental care. In addition, NPY is a

widely distributed neuromodulator that is involved in the regulation of many other physiological processes, as well as behaviors including stress, reproduction, and aggression. Thus, investigation of potential changes in mRNA expression at finer-scale neuroanatomical resolution is needed.

Lastly, levels of *cart2* and *cart4* mRNA also did not differ between gravid and brooding *A. burtoni* females. *cart2* and *cart4* were selected as potential candidates regulating energy balance and feeding behavior because of their previously described role in zebrafish. For example, starvation in zebrafish led to a reduction in the population of *cart2* mRNA-expressing cells of the E and NRL, and in the *cart4* mRNA-expressing cells of the NLT (Akash et al., 2014). However, our observations that hypothalamic *pomc1a* and *cart* mRNA levels do not differ between gravid and brooding females could suggest that regulation of the melanocortin receptors is primarily due to an increase in *agrp* biosynthesis rather than a decrease in *pomc1a* and *cart* biosynthesis. It is important to note, however, that mouth brooding is an extreme form of parental care and forced starvation, and there may be additional regulatory circuitry within the hypothalamus that is fundamentally different from that found in non-brooding fish species in a fasted condition. Further, in mammals, a neural circuit has been identified from the parabrachial nucleus (PBN) to the central nucleus of the amygdala (CeAlc) that mediates appetite suppression during unfavorable conditions, which is different from the circuit that controls appetite suppression after feeding (Carter, Soden, Zweifel, & Palmiter, 2013). Therefore, it would be important in the future to include a starved female group (non-brooding state) with a brooding female group (unfavorable condition). Grone et al. (2012) found that food deprivation accounted for the

physiological changes seen in mouth brooding females (delayed ovarian cycles and subsequent spawning, decrease in body mass), but that starvation alone did not account for the neurological changes. Thus, the starved female group (non-brooding state) could help to determine whether the conditions of the starvation state influences somata sizes and gene expression within specific brain nuclei and whether or not they are due to the parental behavioral state. In addition, it is possible that some neuromolecular mechanisms used for energy storage during the gravid phase are sufficient to support the starvation period during brooding, and are therefore not reflected in mRNA changes. Nevertheless, since these candidate neuropeptides and their functions are relatively well conserved, our work provides insights for understanding the neural control of feeding and reproductive circuits across vertebrate taxa.

CONCLUSIONS

In this study, we provide the first complete distribution patterns of CART, NPY, and AGRP neurons throughout the entire brain of a mouth brooding teleost fish. The similarity in localization of these neuropeptides amongst teleosts, as well as with that of mammals, suggests that the neural circuitries regulating the interaction of feeding and reproduction are relatively well conserved. Reproductive- and metabolic-state plasticity in the somata size of NPY, AGRP, and *pomc1a*-expressing neurons in the *A. burtoni* brain also suggests that these neuropeptides are involved in regulating phenotypic and metabolic changes associated with the transitions between gravidity and mouth brooding parental care stages. Future studies should focus on the functional roles of

these neuropeptides in regulating and maintaining reproductive and metabolic homeostasis during this transition between gravid and mouth brooding states.

ACKNOWLEDGEMENTS

We thank the reviewers and editors for helpful comments to improve the manuscript, Dr. Brian Grone for technical assistance and for providing valuable insights on the project, and members of the Maruska Lab for discussions and fish care.

CONFLICT OF INTEREST STATEMENT

The authors have no known or potential conflicts of interest.

ROLE OF AUTHORS

All authors had full access to the data, take responsibility for the integrity of the data and accuracy of the data analysis, and approved the final manuscript. Designed experiments: KPM and DTP. Performed experiments, collected and analyzed data: DTP, DAR, and KPM. Wrote and edited the article: DTP, DAR, and KPM. Provided funding, equipment, reagents, and supplies: KPM.

LITERATURE CITED

Agulleiro, M. J., Cortes, R., Leal, E., Rios, D., Sanchez, E., & Cerda-Reverter, J. M. (2014). Characterization, tissue distribution and regulation by fasting of the agouti family of peptides in the sea bass (Dicentrarchus labrax). [Research Support, Non-U.S. Gov't]. *Gen Comp Endocrinol, 205*, 251-259. doi: 10.1016/j.ygcen.2014.02.009

Akash, G., Kaniganti, T., Tiwari, N. K., Subhedar, N. K., & Ghose, A. (2014). Differential distribution and energy status-dependent regulation of the four CART neuropeptide genes in the zebrafish brain. [Research Support, Non-U.S. Gov't]. *J Comp Neurol, 522*(10), 2266-2285. doi: 10.1002/cne.23532

Amano, M., Takahashi, A., Yamanome, T., Oka, Y., Amiya, N., Kawauchi, H., & Yamamori, K. (2005). Immunocytochemical localization and ontogenic development of alpha-melanocyte-stimulating hormone (alpha-MSH) in the brain of a pleuronectiform fish, barfin flounder. [Research Support, Non-U.S. Gov't]. *Cell Tissue Res, 320*(1), 127-134. doi: 10.1007/s00441-004-1058-4

Barsagade, V. G., Mazumdar, M., Singru, P. S., Thim, L., Clausen, J. T., & Subhedar, N. (2010). Reproductive phase-related variations in cocaine- and amphetamine-regulated transcript (CART) in the olfactory system, forebrain, and pituitary of the female catfish, Clarias batrachus (Linn.). [Research Support, Non-U.S. Gov't]. *J Comp Neurol, 518*(13), 2503-2524. doi: 10.1002/cne.22349

Batten, T. F., Cambre, M. L., Moons, L., & Vandesande, F. (1990). Comparative distribution of neuropeptide-immunoreactive systems in the brain of the green molly, *Poecilia latipinna*. *Journal of Comparative Neurology, 302*(4), 893-919.

Bogus-Nowakowska, K., Robak, A., Rowniak, M., Wasilewska, B., Najdzion, J., Kolenkiewicz, M., . . . Majewski, M. (2011). Distribution and chemical coding pattern of the cocaine- and amphetamine-regulated transcript (CART) immunoreactivity in the preoptic area of the pig. *Folia Histochem Cytobiol, 49*(4), 604-614.

Boswell, T., Millam, J. R., Li, Q., & Dunn, I. C. (1998). Cellular localization of neuropeptide Y mRNA and peptide in the brain of the Japanese quail and domestic chicken. [Comparative Study

Research Support, Non-U.S. Gov't]. *Cell Tissue Res, 293*(1), 31-38.

Burmeister, S. S., Munshi, R. G., & Fernald, R. D. (2009). Cytoarchitecture of a cichlid fish telencephalon. *Brain Behav Evol, 74*(2), 110-120. doi: 000235613 [pii]
10.1159/000235613

Bustin, S. A., Benes, V., Nolan, T., & Pfaffl, M. W. (2005). Quantitative real-time RT-PCR--a perspective. *J Mol Endocrinol, 34*(3), 597-601. doi: 34/3/597 [pii]
10.1677/jme.1.01755

Butler, J. M., & Maruska, K. P. (2016). The Mechanosensory Lateral Line System Mediates Activation of Socially-Relevant Brain Regions during Territorial Interactions. *Front Behav Neurosci, 10*, 93. doi: 10.3389/fnbeh.2016.00093

Calisi, R. M., Diaz-Munoz, S. L., Wingfield, J. C., & Bentley, G. E. (2011). Social and breeding status are associated with the expression of GnIH. [Research Support, Non-U.S. Gov't

Research Support, U.S. Gov't, Non-P.H.S.]. *Genes Brain Behav, 10*(5), 557-564. doi: 10.1111/j.1601-183X.2011.00693.x

Carter, M. E., Soden, M. E., Zweifel, L. S., & Palmiter, R. D. (2013). Genetic identification of a neural circuit that suppresses appetite. [Research Support, N.I.H., Extramural

Research Support, Non-U.S. Gov't]. *Nature, 503*(7474), 111-114. doi: 10.1038/nature12596

Cerda-Reverter, J. M., Agulleiro, M. J., R, R. G., Sanchez, E., Ceinos, R., & Rotllant, J. (2011). Fish melanocortin system. [Research Support, Non-U.S. Gov't

Review]. *Eur J Pharmacol, 660*(1), 53-60. doi: 10.1016/j.ejphar.2010.10.108

Cerda-Reverter, J. M., Anglade, I., Martinez-Rodriguez, G., Mazurais, D., Munoz-Cueto, J. A., Carrillo, M., . . . Zanuy, S. (2000). Characterization of neuropeptide Y expression in the brain of a perciform fish, the sea bass (Dicentrarchus labrax). *J Chem Neuroanat, 19*(4), 197-210.

Cerda-Reverter, J. M., & Peter, R. E. (2003). Endogenous melanocortin antagonist in fish: structure, brain mapping, and regulation by fasting of the goldfish agouti-related protein gene. [Research Support, Non-U.S. Gov't]. *Endocrinology, 144*(10), 4552-4561. doi: 10.1210/en.2003-0453

Chiba, A., Oka, S., & Honma, Y. (1996). Ontogenetic changes in neuropeptide Y-like-immunoreactivity in the terminal nerve of the chum salmon and the cloudy dogfish, with special reference to colocalization with gonadotropin-releasing hormone-immunoreactivity. *Neurosci Lett, 213*(1), 49-52. doi: 0304394096128287 [pii]

Clutton-Brock, T. H., & Vincent, A. C. (1991). Sexual selection and the potential reproductive rates of males and females. [Comparative Study]. *Nature, 351*(6321), 58-60. doi: 10.1038/351058a0

Copeland, D. L., Duff, R. J., Liu, Q., Prokop, J., & Londraville, R. L. (2011). Leptin in teleost fishes: an argument for comparative study. *Front Physiol, 2*, 26. doi: 10.3389/fphys.2011.00026

Couceyro, P. R., Koylu, E. O., & Kuhar, M. J. (1997). Further studies on the anatomical distribution of CART by in situ hybridization. [Research Support, Non-U.S. Gov't

Research Support, U.S. Gov't, P.H.S.]. *J Chem Neuroanat, 12*(4), 229-241.

Danger, J. M., Breton, B., Vallarino, M., Fournier, A., Pelletier, G., & Vaudry, H. (1991). Neuropeptide-Y in the trout brain and pituitary: localization, characterization, and action on gonadotropin release. [Research Support, Non-U.S. Gov't]. *Endocrinology, 128*(5), 2360-2368. doi: 10.1210/endo-128-5-2360

Daniel, J. A., Foradori, C. D., Whitlock, B. K., & Sartin, J. L. (2013). Hypothalamic integration of nutrient status and reproduction in the sheep. [Review]. *Reprod Domest Anim, 48 Suppl 1*, 44-52. doi: 10.1111/rda.12227

Fernald, R. D., & Hirata, N. R. (1979). The ontogeny of social behavior and body coloration in the African cichlid fish *Haplochromis burtoni*. *Z Tierpsychol, 50*, 180-187.

Forlano, P. M., & Cone, R. D. (2007). Conserved neurochemical pathways involved in hypothalamic control of energy homeostasis. [Research Support, N.I.H., Extramural

Research Support, Non-U.S. Gov't]. *J Comp Neurol, 505*(3), 235-248. doi: 10.1002/cne.21447

Francis, R. C., Soma, K., & Fernald, R. D. (1993). Social regulation of the brain-pituitary-gonadal axis. *Proc. Natl. Acad. Sci. USA, 90*, 7794-7798.

Gaikwad, A., Biju, K. C., Saha, S. G., & Subhedar, N. (2004). Neuropeptide Y in the olfactory system, forebrain and pituitary of the teleost, Clarias batrachus. *J Chem Neuroanat, 27*(1), 55-70.

Grone, B. P., Carpenter, R. E., Lee, M., Maruska, K. P., & Fernald, R. D. (2012). Food deprivation explains effects of mouthbrooding on ovaries and steroid hormones, but not brain neuropeptide and receptor mRNAs, in an African cichlid fish. *Horm Behav, 62*(1), 18-26. doi: S0018-506X(12)00130-4 [pii]
10.1016/j.yhbeh.2012.04.012

Grone, B. P., & Maruska, K. P. (2015). A second corticotropin-releasing hormone gene (CRH2) is conserved across vertebrate classes and expressed in the hindbrain of a basal neopterygian fish, the spotted gar (*Lepisosteus oculatus*). [Research Support, Non-U.S. Gov't]. *J Comp Neurol, 523*(7), 1125-1143. doi: 10.1002/cne.23729

Harris, R. M., Dijkstra, P. D., & Hofmann, H. A. (2014). Complex structural and regulatory evolution of the pro-opiomelanocortin gene family. [Comparative Study
Research Support, Non-U.S. Gov't]. *Gen Comp Endocrinol, 195*, 107-115. doi: 10.1016/j.ygcen.2013.10.007

Hoskins, L. J., & Volkoff, H. (2012). The comparative endocrinology of feeding in fish: insights and challenges. [Research Support, Non-U.S. Gov't
Review]. *Gen Comp Endocrinol, 176*(3), 327-335. doi: 10.1016/j.ygcen.2011.12.025

Hu, C. K., Southey, B. R., Romanova, E. V., Maruska, K. P., Sweedler, J. V., & Fernald, R. D. (2016). Identification of prohormones and pituitary neuropeptides in the African cichlid, Astatotilapia burtoni. *BMC Genomics, 17*(1), 660. doi: 10.1186/s12864-016-2914-9

Imura, K., Yamamoto, N., Sawai, N., Yoshimoto, M., Yang, C. Y., Xue, H. G., & Ito, H. (2003). Topographical organization of an indirect telencephalo-cerebellar pathway through the nucleus paracommissuralis in a teleost, Oreochromis niloticus. *Brain Behav Evol, 61*(2), 70-90.

Kah, O., Pontet, A., Danger, J. M., Dubourg, P., Pelletier, G., Vaudry, H., & Calas, A. (1989). Characterization, cerebral distribution and gonadotropin release activity of neuropeptide Y (NPY) in the goldfish. *Fish Physiol Biochem, 7*(1-6), 69-76. doi: 10.1007/BF00004691

Kong, D., Tong, Q., Ye, C., Koda, S., Fuller, P. M., Krashes, M. J., . . . Lowell, B. B. (2012). GABAergic RIP-Cre neurons in the arcuate nucleus selectively regulate energy expenditure. [Research Support, N.I.H., Extramural
Research Support, Non-U.S. Gov't]. *Cell, 151*(3), 645-657. doi: 10.1016/j.cell.2012.09.020

Koylu, E. O., Couceyro, P. R., Lambert, P. D., & Kuhar, M. J. (1998). Cocaine- and amphetamine-regulated transcript peptide immunohistochemical localization in the rat brain. [Research Support, U.S. Gov't, P.H.S.]. *J Comp Neurol, 391*(1), 115-132.

Lazar, G., Calle, M., Roubos, E. W., & Kozicz, T. (2004). Immunohistochemical localization of cocaine- and amphetamine-regulated transcript peptide in the central nervous system of the frog Rana esculenta. [Comparative Study
Research Support, Non-U.S. Gov't]. *J Comp Neurol, 477*(3), 324-339. doi: 10.1002/cne.20264

Leslie, R. A., Sanders, S. J., Anderson, S. I., Schuhler, S., Horan, T. L., & Ebling, F. J. (2001). Appositions between cocaine and amphetamine-related transcript- and gonadotropin releasing hormone-immunoreactive neurons in the hypothalamus of the Siberian hamster. [Research Support, Non-U.S. Gov't]. *Neurosci Lett, 314*(3), 111-114.

Lin, X., Volkoff, H., Narnaware, Y., Bernier, N. J., Peyon, P., & Peter, R. E. (2000). Brain regulation of feeding behavior and food intake in fish. [Research Support, Non-U.S. Gov't
Review]. *Comp Biochem Physiol A Mol Integr Physiol, 126*(4), 415-434.

Liu, Q., Chen, Y., Copeland, D., Ball, H., Duff, R. J., Rockich, B., & Londraville, R. L. (2010). Expression of leptin receptor gene in developing and adult zebrafish. [Comparative Study
Research Support, N.I.H., Extramural]. *Gen Comp Endocrinol, 166*(2), 346-355. doi: 10.1016/j.ygcen.2009.11.015

Mainen, Z. F., & Sejnowski, T. J. (1996). Influence of dendritic structure on firing pattern in model neocortical neurons. [Research Support, Non-U.S. Gov't]. *Nature, 382*(6589), 363-366. doi: 10.1038/382363a0

Marchetti, G., Cozzi, B., Tavanti, M., Russo, V., Pellegrini, S., & Fabiani, O. (2000). The distribution of neuropeptide Y-immunoreactive neurons and nerve fibers in the forebrain of the carp Cyprinus carpio L. *J Chem Neuroanat, 20*(2), 129-139.

Maruska, K. P. (2014). Social regulation of reproduction in male cichlid fishes. [Research Support, Non-U.S. Gov't]. *Gen Comp Endocrinol, 207*, 2-12. doi: 10.1016/j.ygcen.2014.04.038

Maruska, K. P., Becker, L., Neboori, A., & Fernald, R. D. (2013). Social descent with territory loss causes rapid behavioral, endocrine, and transcriptional changes in the brain. *J Exp Biol*. doi: 10.1242/jeb.088617

Maruska, K. P., Butler, J. M., Field, K. E., & Porter, D. T. (2017). Localization of glutamatergic, GABAergic, and cholinergic neurons in the brain of the African cichlid fish, Astatotilapia burtoni. *J Comp Neurol, 525*(3), 610-638. doi: 10.1002/cne.24092

Maruska, K. P., & Fernald, R. D. (2013). Social Regulation of Male Reproductive Plasticity in an African Cichlid Fish. *Integr Comp Biol, 207*, 2-12. doi: 10.1093/icb/ict017

Maruska, K. P., Levavi-Sivan, B., Biran, J., & Fernald, R. D. (2011). Plasticity of the reproductive axis caused by social status change in an African cichlid fish: I. pituitary gonadotropins. *Endocrinology, 152*, 281-290.

Maruska, K. P., Zhang, A., Neboori, A., & Fernald, R. D. (2013). Social opportunity causes rapid transcriptional changes in the social behavior network of the brain in an African cichlid fish. *J Neuroendocrinol, 25*, 145-157.

Mitter, K., Kotoulas, G., Magoulas, A., Mulero, V., Sepulcre, P., Figueras, A., . . . Sarropoulou, E. (2009). Evaluation of candidate reference genes for QPCR

during ontogenesis and of immune-relevant tissues of European seabass (*Dicentrarchus labrax*). *Comp Biochem Physiol B Biochem Mol Biol, 153*(4), 340-347. doi: S1096-4959(09)00109-2 [pii]
10.1016/j.cbpb.2009.04.009

Mousley, A., Polese, G., Marks, N. J., & Eisthen, H. L. (2006). Terminal nerve-derived neuropeptide y modulates physiological responses in the olfactory epithelium of hungry axolotls (Ambystoma mexicanum). [Research Support, N.I.H., Extramural
Research Support, Non-U.S. Gov't]. *J Neurosci, 26*(29), 7707-7717. doi: 10.1523/JNEUROSCI.1977-06.2006

Mukherjee, A., Subhedar, N. K., & Ghose, A. (2012). Ontogeny of the cocaine- and amphetamine-regulated transcript (CART) neuropeptide system in the brain of zebrafish, Danio rerio. [Research Support, Non-U.S. Gov't]. *J Comp Neurol, 520*(4), 770-797. doi: 10.1002/cne.22779

Munchrath, L. A., & Hofmann, H. A. (2010). Distribution of sex steroid hormone receptors in the brain of an African cichlid fish, *Astatotilapia burtoni*. *J Comp Neurol, 518*(16), 3302-3326. doi: 10.1002/cne.22401

Munoz-Cueto, J. A., Sarasquete, C., Zohar, A. H., & Kah, O. (2001). *An atlas of the brain of the gilthead seabream (Sparus aurata)*. College Park: Maryland Sea Grant.

Murashita, K., Kurokawa, T., Ebbesson, L. O., Stefansson, S. O., & Ronnestad, I. (2009). Characterization, tissue distribution, and regulation of agouti-related protein (AgRP), cocaine- and amphetamine-regulated transcript (CART) and neuropeptide Y (NPY) in Atlantic salmon (Salmo salar). [Research Support, Non-U.S. Gov't]. *Gen Comp Endocrinol, 162*(2), 160-171. doi: 10.1016/j.ygcen.2009.03.015

Nakagawa, S. (2004). A farewell to Bonferroni: the problems of low statistical power and publication bias. *Behav Ecol, 15*(6), 1044-1045.

Navarro, V. M., & Kaiser, U. B. (2013). Metabolic influences on neuroendocrine regulation of reproduction. [Research Support, N.I.H., Extramural
Review]. *Curr Opin Endocrinol Diabetes Obes, 20*(4), 335-341. doi: 10.1097/MED.0b013e32836318ce

O'Connell, L. A., & Hofmann, H. A. (2011). The vertebrate mesolimbic reward system and social behavior network: A comparative synthesis. *J Comp Neurol, 519*, 3599-3639. doi: 10.1002/cne.22735

Pickavance, L. C., Staines, W. A., & Fryer, J. N. (1992). Distributions and colocalization of neuropeptide Y and somatostatin in the goldfish brain. [Research Support, Non-U.S. Gov't]. *J Chem Neuroanat, 5*(3), 221-233.

Pontet, A., Danger, J. M., Dubourg, P., Pelletier, G., Vaudry, H., Calas, A., & Kah, O. (1989). Distribution and characterization of neuropeptide Y-like immunoreactivity in the brain and pituitary of the goldfish. *Cell Tissue Res, 255*(3), 529-538.

Ransdell, J. L., Faust, T. B., & Schulz, D. J. (2010). Correlated Levels of mRNA and Soma Size in Single Identified Neurons: Evidence for Compartment-specific Regulation of Gene Expression. *Front Mol Neurosci, 3*, 116. doi: 10.3389/fnmol.2010.00116

Reiner, A., & Northcutt, R. G. (1992). An immunohistochemical study of the telencephalon of the senegal bichir (Polypterus senegalus). [Research Support,

U.S. Gov't, P.H.S.]. *J Comp Neurol, 319*(3), 359-386. doi: 10.1002/cne.903190305

Renn, S. C., Carleton, J. B., Magee, H., Nguyen, M. L., & Tanner, A. C. (2009). Maternal care and altered social phenotype in a recently collected stock of *Astatotilapia burtoni* cichlid fish. *Integr Comp Biol, 49*(6), 660-673. doi: icp085 [pii]
10.1093/icb/icp085

Ringholm, A., Klovins, J., Fredriksson, R., Poliakova, N., Larson, E. T., Kukkonen, J. P., . . . Schioth, H. B. (2003). Presence of melanocortin (MC4) receptor in spiny dogfish suggests an ancient vertebrate origin of central melanocortin system. [Research Support, Non-U.S. Gov't]. *Eur J Biochem, 270*(2), 213-221.

Roa, J. (2013). Role of GnRH Neurons and Their Neuronal Afferents as Key Integrators between Food Intake Regulatory Signals and the Control of Reproduction. [Review]. *Int J Endocrinol, 2013*, 518046. doi: 10.1155/2013/518046

Roberts, C. B., Best, J. A., & Suter, K. J. (2006). Dendritic processing of excitatory synaptic input in hypothalamic gonadotropin releasing-hormone neurons. [Research Support, N.I.H., Extramural]. *Endocrinology, 147*(3), 1545-1555. doi: 10.1210/en.2005-1350

Rodriguez-Gomez, F. J., Rendon-Unceta, C., Sarasquete, C., & Munoz-Cueto, J. A. (2001). Distribution of neuropeptide Y-like immunoreactivity in the brain of the Senegalese sole (Solea senegalensis). [Research Support, Non-U.S. Gov't]. *Anat Rec, 262*(3), 227-237.

Rondini, T. A., Baddini, S. P., Sousa, L. F., Bittencourt, J. C., & Elias, C. F. (2004). Hypothalamic cocaine- and amphetamine-regulated transcript neurons project to areas expressing gonadotropin releasing hormone immunoreactivity and to the anteroventral periventricular nucleus in male and female rats. [Research Support, Non-U.S. Gov't]. *Neuroscience, 125*(3), 735-748. doi: 10.1016/j.neuroscience.2003.12.045

Sakharkar, A. J., Singru, P. S., Sarkar, K., & Subhedar, N. K. (2005). Neuropeptide Y in the forebrain of the adult male cichlid fish *Oreochromis mossambicus*: distribution, effects of castration and testosterone replacement. *J Comp Neurol, 489*(2), 148-165.

Sanchez, E., Rubio, V. C., & Cerda-Reverter, J. M. (2009). Characterization of the sea bass melanocortin 5 receptor: a putative role in hepatic lipid metabolism. [Research Support, Non-U.S. Gov't]. *J Exp Biol, 212*(Pt 23), 3901-3910. doi: 10.1242/jeb.035121

Schioth, H. B., & Watanobe, H. (2002). Melanocortins and reproduction. [Research Support, Non-U.S. Gov't
Review]. *Brain Res Brain Res Rev, 38*(3), 340-350.

Schneider, J. E. (2004). Energy balance and reproduction. [Research Support, U.S. Gov't, Non-P.H.S.
Review]. *Physiol Behav, 81*(2), 289-317. doi: 10.1016/j.physbeh.2004.02.007

Shahjahan, M., Kitahashi, T., & Parhar, I. S. (2014). Central pathways integrating metabolism and reproduction in teleosts. [Review]. *Front Endocrinol (Lausanne), 5*, 36. doi: 10.3389/fendo.2014.00036

Singru, P. S., Mazumdar, M., Sakharkar, A. J., Lechan, R. M., Thim, L., Clausen, J. T., & Subhedar, N. K. (2007). Immunohistochemical localization of cocaine- and amphetamine-regulated transcript peptide in the brain of the catfish, Clarias batrachus (Linn.). *J Comp Neurol, 502*(2), 215-235.

Sohn, J. W., Elmquist, J. K., & Williams, K. W. (2013). Neuronal circuits that regulate feeding behavior and metabolism. [Research Support, N.I.H., Extramural
Research Support, Non-U.S. Gov't
Review]. *Trends Neurosci, 36*(9), 504-512. doi: 10.1016/j.tins.2013.05.003

Song, Y., Golling, G., Thacker, T. L., & Cone, R. D. (2003). Agouti-related protein (AGRP) is conserved and regulated by metabolic state in the zebrafish, Danio rerio. [Research Support, Non-U.S. Gov't]. *Endocrine, 22*(3), 257-265. doi: 10.1385/ENDO:22:3:257

Sternson, S. M., & Atasoy, D. (2014). Agouti-related protein neuron circuits that regulate appetite. [Review]. *Neuroendocrinology, 100*(2-3), 95-102. doi: 10.1159/000369072

Subhedar, N., Cerda, J., & Wallace, R. A. (1996). Neuropeptide Y in the forebrain and retina of the killifish, Fundulus heteroclitus. [Research Support, Non-U.S. Gov't
Research Support, U.S. Gov't, Non-P.H.S.]. *Cell Tissue Res, 283*(2), 313-323.

Subhedar, N. K., Nakhate, K. T., Upadhya, M. A., & Kokare, D. M. (2014). CART in the brain of vertebrates: circuits, functions and evolution. [Research Support, Non-U.S. Gov't
Review]. *Peptides, 54*, 108-130. doi: 10.1016/j.peptides.2014.01.004

Tena-Sempere, M. (2007). Roles of ghrelin and leptin in the control of reproductive function. [Research Support, Non-U.S. Gov't]. *Neuroendocrinology, 86*(3), 229-241. doi: 10.1159/000108410

True, C., Verma, S., Grove, K. L., & Smith, M. S. (2013). Cocaine- and amphetamine-regulated transcript is a potent stimulator of GnRH and kisspeptin cells and may contribute to negative energy balance-induced reproductive inhibition in females. [Research Support, N.I.H., Extramural
Research Support, Non-U.S. Gov't]. *Endocrinology, 154*(8), 2821-2832. doi: 10.1210/en.2013-1156

Volkoff, H., Canosa, L. F., Unniappan, S., Cerda-Reverter, J. M., Bernier, N. J., Kelly, S. P., & Peter, R. E. (2005). Neuropeptides and the control of food intake in fish. [Research Support, Non-U.S. Gov't
Review]. *Gen Comp Endocrinol, 142*(1-2), 3-19. doi: 10.1016/j.ygcen.2004.11.001

Wade, G. N., & Jones, J. E. (2004). Neuroendocrinology of nutritional infertility. [Research Support, U.S. Gov't, P.H.S.
Review]. *Am J Physiol Regul Integr Comp Physiol, 287*(6), R1277-1296. doi: 10.1152/ajpregu.00475.2004

Wan, Y., Zhang, Y., Ji, P., Li, Y., Xu, P., & Sun, X. (2012). Molecular characterization of CART, AgRP, and MC4R genes and their expression with fasting and re-feeding in common carp (Cyprinus carpio). [Comparative Study
Research Support, Non-U.S. Gov't]. *Mol Biol Rep, 39*(3), 2215-2223. doi: 10.1007/s11033-011-0970-4

Williams, K. W., & Elmquist, J. K. (2012). From neuroanatomy to behavior: central integration of peripheral signals regulating feeding behavior. [Research Support, N.I.H., Extramural
Research Support, Non-U.S. Gov't
Review]. *Nat Neurosci, 15*(10), 1350-1355. doi: 10.1038/nn.3217

Wullimann, M. F., Rupp, B., & Reichert, H. (1996). *Neuroanatomy of the zebrafish brain: a topological atlas*. Basel, Switzerland: Birkhauser Verlag.

Yan, P., Jia, J., Yang, G., Wang, D., Sun, C., & Li, W. (2017). Duplication of neuropeptide Y and peptide YY in Nile tilapia Oreochromis niloticus and their roles in food intake regulation. *Peptides, 88*, 97-105. doi: 10.1016/j.peptides.2016.12.010

Yang, Y., Atasoy, D., Su, H. H., & Sternson, S. M. (2011). Hunger states switch a flip-flop memory circuit via a synaptic AMPK-dependent positive feedback loop. [Research Support, Non-U.S. Gov't]. *Cell, 146*(6), 992-1003. doi: 10.1016/j.cell.2011.07.039

Yokobori, E., Azuma, M., Nishiguchi, R., Kang, K. S., Kamijo, M., Uchiyama, M., & Matsuda, K. (2012). Neuropeptide Y stimulates food intake in the Zebrafish, Danio rerio. [Research Support, Non-U.S. Gov't]. *J Neuroendocrinol, 24*(5), 766-773. doi: 10.1111/j.1365-2826.2012.02281.x

Yu, K. L., Rosenblum, P. M., & Peter, R. E. (1991). In vitro release of gonadotropin-releasing hormone from the brain preoptic-anterior hypothalamic region and pituitary of female goldfish. [Research Support, Non-U.S. Gov't]. *Gen Comp Endocrinol, 81*(2), 256-267.

Zahid, M., Malik, S., & Rani, S. (2014). Neuropeptide Y (NPY) distribution in the forebrain of adult spiny eel, *Macrognathus pancalus*. *J Endocrinol, 2*, 75-86.

Zhang, C., Forlano, P. M., & Cone, R. D. (2012). AgRP and POMC neurons are hypophysiotropic and coordinately regulate multiple endocrine axes in a larval teleost. [Research Support, N.I.H., Extramural]. *Cell Metab, 15*(2), 256-264. doi: 10.1016/j.cmet.2011.12.014

Zhao, S., & Fernald, R. D. (2005). Comprehensive algorithm for quantitative real-time polymerase chain reaction. *J Comput Biol, 12*(8), 1047-1064.

Zohar, Y., Munoz-Cueto, J. A., Elizur, A., & Kah, O. (2010). Neuroendocrinology of reproduction in teleost fish. [Review]. *Gen Comp Endocrinol, 165*(3), 438-455. doi: 10.1016/j.ygcen.2009.04.017

Abbreviations

4v	fourth ventricle
ac	anterior commissure
aGn	anterior glomerular nucleus
An	anterior thalamic nucleus
AP	accessory pretectal nucleus
ATn	anterior tuberal nucleus
Cc	central canal
CC	cerebellar crest
CCeG	granular layer of corpus cerebelli
CCeM	molecular layer of corpus cerebelli
CCeP	Purkinje cell layer of corpus cerebelli
CG	central gray
CM	corpus mammillare
CP	central posterior thalamic nucleus
CTn	central thalamic nucleus
CZ	central zone of tectum
DAO	dorsal accessory optic nucleus
Dc	central part of the dorsal telencephalon
Dc-1	central part of the dorsal telencephalon, subdivision 1
Dc-2	central part of the dorsal telencephalon, subdivision 2
Dc-3	central part of the dorsal telencephalon, subdivision 3
Dc-4	central part of the dorsal telencephalon, subdivision 4
Dc-5	central part of the dorsal telencephalon, subdivision 5
Dd	dorsal part of the dorsal telencephalon
Dd-d	dorsal part of the dorsal telencephalon, dorsal subdivision
Dl	lateral part of the dorsal telencephalon
Dl-d	dorsal part of lateral part of the dorsal telencephalon
Dl-g	granular zone of lateral part of the dorsal telencephalon
Dl-v1	ventral part of the lateral part of the dorsal telencephalon, subdivision 1
Dl-v2	ventral part of the lateral part of the dorsal telencephalon, subdivision 2
Dm	medial part of the dorsal telencephalon
Dm-1	medial part of the dorsal telencephalon, subdivision 1
Dm-2c	medial part of the dorsal telencephalon, caudal subdivision 2
Dm-2r	medial part of the dorsal telencephalon, rostral subdivision 2
Dm-3	medial part of the dorsal telencephalon, subdivision 3
DON	descending octavolateralis nucleus
Dp	posterior part of the dorsal telencephalon
DP	dorsal posterior thalamic nucleus
dtt	descending trigeminal tract
DT	dorsal tegmental nucleus
DWZ	deep white zone of tectum
Dx	unassigned subdivision of dorsal telencephalon
E	entopeduncular nucleus
ECL	external cell layer of olfactory bulb
EG	granular eminence

fr	fasciculus retroflexus
GL	glomerular layer of olfactory bulb
Gn	glomerular nucleus
gTN	ganglion of the terminal nerve
hc	horizontal commissure
IC	intercalated nucleus
ICL	inner cell layer of olfactory bulb
ICo	isthmic commissure
IIIn	oculomotor nucleus
IO	inferior olive
IP	interpeduncular nucleus
IVn	trochlear nucleus
LC	locus coeruleus
LFB	lateral forebrain bundle
LFN	lateral funicular nucleus
LL	lateral lemniscus
LT	lateral tegmental nucleus
MFN	medial funicular nucleus
mlf	medial longitudinal fasciculus
MON	medial octavolateralis nucleus
NC	nucleus corticalis
NCIL	central nucleus of the inferior lobe
NDILc	caudal part of the diffuse nucleus of the inferior lobe
NDILl	lateral part of the diffuse nucleus of the inferior lobe
NDILm	medial part of the diffuse nucleus of the inferior lobe
nGMp	magnocellular preoptic nucleus, gigantocellular division
nHd	dorsal habenular nucleus
nHv	ventral habenular nucleus
NI	nucleus isthmi
NLL	nucleus of the lateral lemniscus
NLT	lateral tuberal nucleus
NLTd	lateral tuberal nucleus, dorsal part
NLTi	lateral tuberal nucleus, intermediate part
NLTl	lateral tuberal nucleus, lateral part
NLTm	lateral tuberal nucleus, medial part
NLTv	lateral tuberal nucleus, ventral part
NLVa	anterior part of nucleus of the lateral valvulae
NLVc	central part of nucleus of the lateral valvulae
NMIL	medial nucleus of the interior lobe
nMLF	nucleus of medial longitudinal fasciculus
nMMp	magnocellular preoptic nucleus, magnocellular division
NP	nucleus pretectalis
NPC	central pretectal nucleus
nPPa	parvocellular preoptic nucleus, anterior part
nPMp	magnocellular preoptic nucleus, parvocellular division
nPPp	parvocellular preoptic nucleus, posterior part

NPT	posterior tuberal nucleus
NR	nucleus ruber
NRL	nucleus of the lateral recess
NRP	nucleus of the posterior recess
NT	nucleus taenia
nTE	nucleus of the thalamic eminentia
OEN	octavolateralis efferent nucleus
ON	optic nerve
PAG	periaqueductal gray
pc	posterior commissure
PGc	commissural preglomerular nucleus
PGm	medial preglomerular nucleus
PGn	preglomerular nucleus
Pgd	dorsal preglomerular nucleus
PGl	lateral preglomerular nucleus
PGm	medial preglomerular nucleus
PGZ	periventricular gray zone of tectum
Pit	pituitary
PLm	medial part of the perilemniscular nucleus
PN	prethalamic nucleus
PPd	dorsal periventricular pretectal nucleus
PPv	ventral part of the periventricular pretectal nucleus
PS	pineal stalk
PSi	superficial pretectal nucleus, intermediate division
PSm	superficial pretectal nucleus, medial division
PSP	parvocellular superficial pretectal nucleus
PT	posterior thalamic nucleus
PTN	posterior tuberal nucleus
PTT	paratoral tegmental nucleus
PVO	paraventricular organ
Ri	inferior reticular nucleus
Rm	medial reticular nucleus
Rs	superior reticular formation
SGn	secondary gustatory nucleus
sgt	secondary gustatory tract
SOF	secondary olfactory layer of olfactory bulb
SR	superior raphe nucleus
SVn	secondary visceral nucleus
SWGZ	superficial gray and white zone of tectum
T	tectum
TBT	tectobulbar tract
TGN	tertiary gustatory nucleus
TL	torus longitudinalis
TLa	torus lateralis
TMCa	anterior mesencephalocerebellar tract
TMCp	posterior mesencephalocerebellar tract

TPp	periventricular nucleus of posterior tuberculum
TS	torus semicircularis
TSc	central nucleus of torus semicircularis
TSvl	ventrolateral nucleus of torus semicircularis
VAO	ventral accessory optic nucleus
Vc	central part of the ventral telencephalon
VCeG	granular layer of valvula cerebelli
VCeM	molecular layer of valvula cerebelli
VCeP	Purkinje layer of valvula cerebelli
Vd	dorsal part of the ventral telencephalon
Vd-c	dorsal part of the ventral telencephalon, caudal subdivision
Vd-r	dorsal part of the ventral telencephalon, rostral subdivision
Vde	descending tract of the trigeminal nerve
VH	ventral horn
Vi	intermediate nucleus of the ventral telencephalon
Vl	lateral part of the ventral telencephalon
VL	Vagal lobe
VLn	ventrolateral thalamic nucleus
VIIm	facial motor nucleus
VIIs	facial sensory nucleus
VMn	ventromedial thalamic nucleus
VOT	ventral optic tract
Vp	postcommissural nucleus of the ventral telencephalon
Vs	supracommissural nucleus of the ventral telencephalon
Vs-l	lateral part of the supracommissural nucleus of the ventral telencephalon
Vs-m	medial part of the supracommissural nucleus of the ventral telencephalon
Vv	ventral nucleus of the ventral telencephalon
Xm	vagal motor nucleus

FIGURE LEGENDS

Figure 1. Photomicrographs showing antibody specificity for NPY, AGRP and CART, and specificity of probe binding for *npy, agrp, cart2, cart4, and pomc1a* in the brain of *Astatotilapia burtoni* females. Representative coronal sections showing typical positive staining along with adjacent control alternate sections stained with preabsorbed antibody (IHC) or sense probes (ISH) for NPY IHC (**A-B**), *npy* ISH (**C-D**), AGRP IHC (**E-F**), *agrp* ISH (**G-H**), CART IHC (**I-J**), *cart4* ISH (**K-L**), *cart2* ISH (**M-N**) and *pomc1a* ISH (**O-P**). S, sense; AS, anti-sense. Scale bars = 25 μm in A-B, E-F, and I-J; 50 μm in C-D, G-H, K-L, M-N, O-P. See list for abbreviations.

Figure 2. Representative photomicrographs of alternate sections stained via immunohistochemistry (IHC) and *in situ* hybridization (ISH) for candidate neuropeptides in the brain of *Astatotilapia burtoni*. AGRP antibody (**A**) and *agrp* ISH probe (**B**) both label cells in the NLTv (arrows). NPY antibody labels cells in Vl, but only shows fibers in Vv (**C**). *npy* ISH shows labeled cells in Vl similar to the antibody, but also reveals *npy*-expressing cells in Vv (**D**), as well as many other regions (see Methods and Results). The CART antibody labels large cells in DT (**E**), which are also detected via *cart4* ISH (**F**). However, the CART antibody also labels large neurons in nMLF along the midline, which are not detected by *cart4* ISH. An additional small cell population consistently observed in the tegmentum also contains *cart4*-expressing cells (arrowhead) that is not detected by the antibody. CART antibody also labels cells in Vc (**G**), which are also detected with *cart2* ISH (**H**). Scale bars = 50 μm (A-D, G, H) and 100 μm (E,F).

Figure 3. Brain regions used for somata size measurements and qPCR. Caudal (**A**) to rostral (**D**) transverse sections showing NLT regions (NLTd, NLTi, NLTm, NLTv; shaded gray) of the hypothalamus. Somata size measurements were taken for AGRP, NPY, and *pomc1a* from the NLTv, NLTi, and NLTm throughout the rostro-caudal extent shown. Left side shows cresyl violet stained section and right side shows traced nuclei. Scale bars (A-D) = 250 μm. Approximate location of each transverse section is indicated on **E**. Hypothalamic tissue (shaded gray in **E**) used for qPCR analysis was macro-dissected via cuts (lines) at the locations indicated on the sagittal brain illustration shown in **E**. See list for abbreviations.

Figure 4. Physiological differences between gravid and mouth brooding *Astatotilapia burtoni* females. Gravid females have greater gonadosomatic index (GSI) (**A**), ova diameters (**B**), hepatosomatic index (HSI) (**C**), and condition factors (**D**) compared to brooding females. In each graph, the bottom of each box is the 25th percentile, the top is the 75th percentile and the line in the middle is the median. Whiskers (error bars) indicate the 10th and 90th percentiles and dots represent points outside the 10th-90th percentile. N=12 for both gravid and brooding females for A-D. Different letters indicate statistical differences at $p<0.05$.

Figure 5. Localization of neuropeptide Y (NPY)-immunoreactive neurons in the brain of *Astatotilapia burtoni*. Representative line drawings of transverse sections from rostral (**A**) to caudal (**N**) brain regions show the locations of NPY ir-somata (large

black dots) and fibers (small black dots). Left side of brain shows NPY distribution and right side shows labels of nuclei and other neuroanatomical structures. Figure inset at the top right shows a lateral view of the brain indicating the approximate location of each transverse section. Scale bar = 250 μm. See list for abbreviations.

Figure 6. Representative photomicrographs of NPY-immunoreactive somata and fibers in the brain of *Astatotilapia burtoni*. Coronal sections showing NPY-ir cells in gTN (**A**). NPY-ir cells in the region between Dc-4 and Dc-5 (arrowhead) (**B**). Cells and fibers in the Vc and Vl (**C**) and entopeduncular nucleus (**D**). NPY-ir fibers in the nPPa (**E**). In the diencephalon, NPY-ir cells and fibers are found in the ATn and NLTd of the hypothalamus (arrowheads) (**F-G**). Large NPY-ir cells in DT and ventrally projecting varicose fibers (arrowhead) (**H**). Scale bars = 50 μm B, C; 25 μm in A, E, F; 10 μm in D, G, H. See list for abbreviations.

Figure 7. Representative photomicrographs of *npy*–expressing cells in the brain of *Astatotilapia burtoni*. Cells are abundant in the ICL of the olfactory bulb (A), and in subpallial nuclei of the ventral telencephalon, including Vv, Vl, Vc, Vd, Vs-m, and Vp (**B-C**). *npy* cells also lie in preoptic nuclei nPPa, nPPp, and nMMp, as well as nTE (**C-D**). Cells lie in the PVO, ATn, and NLTv regions, as well as the PGZ of the tectum, and TSc (**E**). In the rhombencephalon, *npy*-expressing cells are found in the SGn, SVn, IO, Ri, and MFN of the rostral spinal cord (**F-H**). Scale bars = 100 μm (A, D, F, H), 250 μm (B, C, E), 50 μm (G).

Figure 8. Localization of AGRP (left half)- and CART (right half)-immunoreactivity in the brain of *Astatotilapia burtoni*. Representative line drawings of transverse sections from rostral (**A**) to caudal (**M**) brain regions show the locations of AGRP and CART ir-somata (large black dots) and fibers (small black dots). Left side of brain shows AGRP distribution and right side shows CART distribution, along with labels of nuclei and other neuroanatomical structures. Figure inset at the top right shows a lateral view of the brain indicating the approximate levels of the corresponding transverse sections. Scale bar = 250 μm. See list for abbreviations.

Figure 9. Representative photomicrographs of AGRP-immunoreactive somata and fibers in the brain of *Astatotilapia burtoni*. Coronal sections of the diencephalon show immunoreactive fibers in Vv (**A**). Moderately dense fibers (arrowheads) in nPPp (**B**). Immunoreactive fibers with large varicosities (arrowheads) in NLTv of the hypothalamus (**C**). AGRP-ir cells (arrowheads) and fibers in NLTv (**D**). Scattered fibers (arrowheads) are present in the NRL surrounding the lateral recess (**E**), and in the ATn (**F**). Scale bars = 25 μm in A, B, E; 10 μm in C, D; 50 μm in F. See list for abbreviations.

Figure 10. Representative photomicrographs of CART-immunoreactive somata and fibers in the brain of *Astatotilapia burtoni*. Coronal sections of the telencephalon show CART-ir cells (arrowheads) in the Vc (**A**) and entopeduncular nucleus (**B**). Small CART-ir cells in Vv (**C**). Immunoreactive cells (arrowheads) in the nPPp (**D**) and NLTv (**E**). A group of small CART-ir cells lies in the thalamus adjacent to DP (**F**). CART-ir cells in NRP (**G**). Large immunoreactive cells are also present in DT and along the midline in

nMLF (**H**) of the mesencephalon. Scale bars = 25 μm in A, B, D; 50 μm in C, F, H; 10 μm in G, E. See list for abbreviations.

Figure 11. Representative photomicrographs of *cart4*–expressing cells in the brain of *Astatotilapia burtoni*. *cart4* cells in the habenula (nHd), and thalamic VMn and IC (**A-C**). Cluster of large cells in DT (**D**). In the hindbrain, *cart4* cells are found in the CG and Ri (**E-F**). Scale bars = 100 μm (A, C, D, F), 50 μm (B, E).

Figure 12. Representative photomicrographs of *cart2*–expressing cells in the brain of *Astatotilapia burtoni*. *cart2*-expressing cells are abundant in the ICL of the olfactory bulb (**A**). In the telencephalon, numerous *cart2* cells lie in subpallial Vc/Vl, Vv, and Vi regions, as well as pallial Dc-3, -4, and -5 (**B-E**). *cart2* cells are expressed in preoptic nuclei nPPa, nPPp, and nMMp (**C,E**). *cart2* cells in the PPd, PPv, TPp, ATn, and PGm (**F**). Cells lie in several diencephalic and mesencephalic regions, including PT, TLa, TSc, and NRL, and cells surround some nuclei such as PGm (**G**). The ATn and NLTv have *cart2*-expressing cells (**H**). Cells lie in TSc, LT, CM, and NMIL, and cells surround Gn and PGn (**I**). *cart2* cells also lie in the PGZ of the tectum, SGn, SVn, LC, SR, and Rs (J). In the rhombencephalon, *cart2*-expressing cells are found in the sensory vagal lobe (VL) and MFN of the rostral spinal cord (**K-L**). Scale bars = 100 μm (A, D, E, H, K, L), 250 μm (B, C, F, G, I, J).

Figure 13. Reproductive state differences in somata sizes of AGRP, NPY, and *pomc1a* neurons in the lateral tuberal nucleus of *Astatotilapia burtoni* females.

NPY-ir (**A**) and AGRP-ir (**B**) somata sizes are larger in gravid compared to brooding females, while *pomc1a* (**C**) neurons are larger in brooding compared to gravid females. In each graph, the bottom of each box is the 25th percentile, the top is the 75th percentile and the line in the middle is the median. Whiskers (error bars) indicate the 10th and 90th percentiles and dots represent points outside the 10th-90th percentile. Sample sizes (number of fish analyzed) are indicated beneath each plot. Different letters indicate statistical differences at $p<0.05$. Representative stained transverse sections through the NLT for gravid and brooding females are shown at right. Scale bars = 10 μm.

Table 1. Details of Primary Antibodies Used in This Study

Antigen	Immunogen	Host, Antibody Type, Source, Catalog #, RRID	Dilution
AGRP	Agouti-Related Protein (83-132)-NH2 (Human), immunogenic sequence: Ser-Ser-Arg-Arg-Cys-Val-Arg-Leu-His-Glu-Ser-Cys-Leu-Gly-Gln-Gln-Val-Pro-Cys-Cys-Asp-Pro-Cys-Ala-Thr-Cys-Tyr-Cys-Arg-Phe-Phe-Asn-Ala-Phe-Cys-Tyr-Cys-Arg-Lys-Leu-Gly-Thr-Ala-Met-Asn-Pro-Cys-Ser-Arg-Thr-NH2 [Contains 5 disulfide bridges. Precise positions are undetermined]	Rabbit, Polyclonal; Phoenix Pharmaceuticals #H-003-53; RRID: AB_2313908	1:10,000
CART	CART (55-102), immunogenic sequence: Ile-Pro-Ile-Tyr-Glu-Lys-Lys-Tyr-Gly-Gln-Val-Pro-Met-Cys-Asp-Ala-Gly-Glu-Gln-Cys-Ala-Val-Arg-Lys-Gly-Ala-Arg-Ile-Gly-Lys-Leu-Cys-Asp-Cys-Pro-Arg-Gly-Thr-Ser-Cys-Asn-Ser-Phe-Leu-Leu-Lys-Cys-Leu [Disulfide bonds between Cys 1-Cys 3, Cys 2-Cys 5, Cys 4-Cys 6]	Rabbit, Polyclonal; Phoenix Pharmaceuticals #H-003-62; RRID: AB_2313614	1:5,000
NPY	Synthetic NPY peptide (porcine) conjugated to KLH	Rabbit, Polyclonal; Sigma Aldrich N9528; RRID: AB_260814	1:12,000

Table 2. Primer Sequences Used for qPCR and to Generate Templates for Synthesis of Riboprobes for *in situ* Hybridization

Primer Sequences for qPCR

Gene	Forward (5'→3')	Reverse (5'→3')
pomc1a	ACAGATCCAATCAGCCTTTC	GACCACTCTCTTTCCCTTTG
npy	CCTTGACGGAGGCATACCC	GAGGTTGATGTAATGTCTCAGC
agrp	GGATTCTGGTGCTGCTAAA	CATCGAGCATTCGGTGAA
cart2	CCCACCCACTTTATGTCAGTAG	CTGAGACTTTACAGCGTGTATG
cart4	CAATCGTCTCGCTCCATATT	CCGTGCAGCTTTATGAAGAA
lepr	CGGGAGAAGGACTTGTATTATC	GCTCCACTTTGGCTTCTT
ghs-r1	CGTGTCTCACAGGGATAAGA	TAGCGACCCACATGGAAA

Primer Sequences for Riboprobes*

pomc1a	GGCAGGTGCAGATGCACACAGAGAATG	AGCTCTTCATGACCCCGCCGTAAC
npy	CAAGCGCTCAGAAGAGAAA	CACAGATGACGACTCAGAATAA
agrp	CACTGAAACCTCCTTCCTATC	GCACAATCCACACATAGATTTC
cart2	GTGGAGCGACTATTTGAGAC	TCGCCACCATCCTTACA
cart4	CAGACACCACAGAAGAAGAG	GAGCCGTGCAGCTTTAT

*T3 transcription initiation sequence (aattaaccctcactaaaggg) was added to the reverse primer (for antisense probes) or forward primer (for sense control probes) for riboprobes.

Table 3. Correlations Between Somata Sizes (NPY, AGRP, *pomc1a*), Gonadosomatic Index (GSI), and Hepatosomatic Index (HSI) for Combined Gravid and Brooding *A. burtoni* Females

	AGRP	*pomc1a*	GSI	HSI
NPY	0.653 **0.001***	-0.7821 **<0.001***	0.659 **0.001***	0.405 0.068
AGRP		-0.696 **0.001***	0.581 **0.005***	0.370 0.09
pomc1a			-0.480 **0.032***	-0.276 0.239

Correlation coefficients (*R*; top) and *P*-values (bottom) are shown. Sample size was 20-22 fish for each comparison (10-11 individuals per reproductive state). *Denotes significance at $P<0.05$ from Pearson Correlation tests.

Table 4. Relative mRNA Levels in the Hypothalamus of Gravid and Mouthbrooding *A. burtoni* Females

Gene	Gravid Females	Mouthbrooding Females	F	df	*P*
agrp	0.0146 ± 0.0153	0.00393 ± 0.00298	4.926	23	**0.037***
cart2	$1.15x10^{-8} \pm 6.20x10^{-9}$	$1.67x10^{-8} \pm 1.14x10^{-8}$	2.284	25	0.143
cart4	$4.0x10^{-10} \pm 8.00x10^{-10}$	$1.00x10^{-10} \pm 2.00x10^{-10}$	1.851	24	0.186
ghs-r1	0.00226 ± 0.000953	0.00345 ± 0.00213	0.023	24	0.880
lepr	0.00226 ± 0.000953	0.00345 ± 0.00213	3.380	23	0.079
npy	$1.99x10^{-8} \pm 9.60x10^{-9}$	$3.32x10^{-8} \pm 2.79x10^{-8}$	3.099	25	0.091
pomc1a	0.00166 ± 0.000783	0.00172 ± 0.00132	0.001	25	0.974

Macro-dissected hypothalamic mRNA levels are normalized to the geometric mean of the reference genes *18s* and *rpl32* (see methods for details). Values are reported as mean ± SD. Statistical values are results of ANCOVA, using hypothalamic mass as a covariate.

Table 5. Correlations Between Hypothalamic mRNA Levels of Candidate Genes for Combined Gravid and Mouth Brooding *A. burtoni* Females

	agrp	***ghs-r1***	***lepr***	***npy***	***cart2***	***cart4***
pomc1a	0.547 **0.004***	0.220 0.281	0.316 0.124	0.233 0.243	-0.0967 0.631	-0.139 0.498
agrp		0.371 0.0678	0.362 0.0822	0.0215 0.917	-0.183 0.371	-0.0347 0.869
ghs-r1			0.281 0.164	0.506 **0.007***	-0.370 0.0572	-0.265 0.191
lepr				0.501 **0.009***	0.167 0.414	-0.0540 0.798
npy					-0.148 0.452	-0.137 0.495
cart2						0.188 0.348

Correlation coefficients (*R*; top) and *P*-values (bottom) are shown. Sample size was 28 fish for each comparison (15 gravid, 13 brooding individuals). *Denotes significance at *P*<0.05 from Pearson Correlation tests.

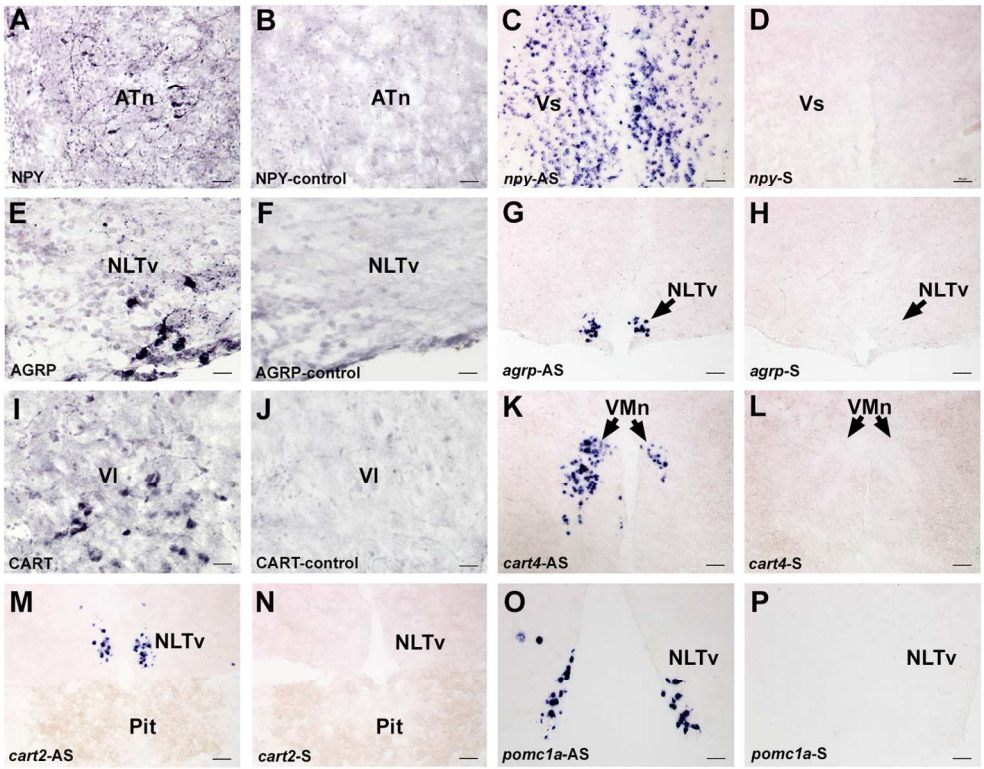

Figure 1. Photomicrographs showing antibody specificity for NPY, AGRP and CART, and specificity of probe binding for npy, agrp, cart2, cart4, and pomc1a in the brain of Astatotilapia burtoni females. Representative coronal sections showing typical positive staining along with adjacent control alternate sections stained with preabsorbed antibody (IHC) or sense probes (ISH) for NPY IHC (A-B), npy ISH (C-D), AGRP IHC (E-F), agrp ISH (G-H), CART IHC (I-J), cart4 ISH (K-L), cart2 ISH (M-N) and pomc1a ISH (O-P). S, sense; AS, anti-sense. Scale bars = 25 μm in A-B, E-F, and I-J; 50 μm in C-D, G-H, K-L, M-N, O-P. See list for abbreviations.

133x105mm (300 x 300 DPI)

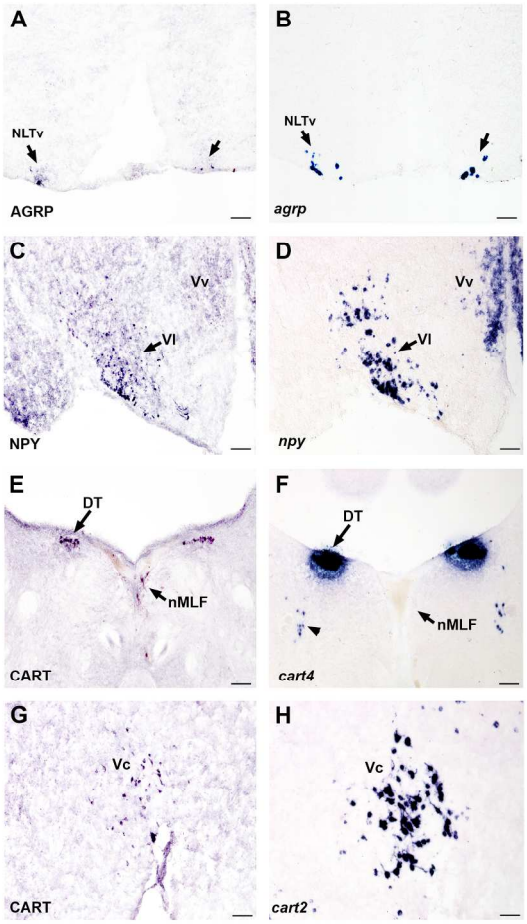

Figure 2. Representative photomicrographs of alternate sections stained via immunohistochemistry (IHC) and in situ hybridization (ISH) for candidate neuropeptides in the brain of Astatotilapia burtoni. AGRP antibody (A) and agrp ISH probe (B) both label cells in the NLTv (arrows). NPY antibody labels cells in Vl, but only shows fibers in Vv (C). npy ISH shows labeled cells in Vl similar to the antibody, but also reveals npy-expressing cells in Vv (D), as well as many other regions (see Methods and Results). The CART antibody labels large cells in DT (E), which are also detected via cart4 ISH (F). However, the CART antibody also labels large neurons in nMLF along the midline, which are not detected by cart4 ISH. An additional small cell population consistently observed in the tegmentum also contains cart4-expressing cells (arrowhead) that is not detected by the antibody. CART antibody also labels cells in Vc (G), which are also detected with cart2 ISH (H). Scale bars = 50 μm (A-D, G, H) and 100 μm (E,F).

203x254mm (300 x 300 DPI)

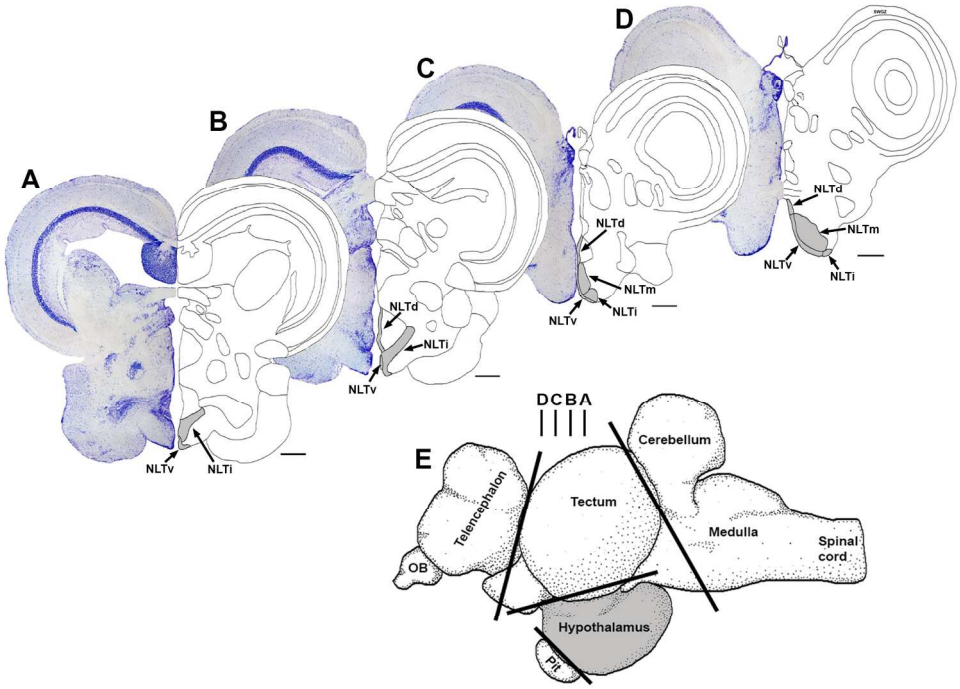

Figure 3. Brain regions used for somata size measurements and qPCR. Caudal (A) to rostral (D) transverse sections showing NLT regions (NLTd, NLTi, NLTm, NLTv; shaded gray) of the hypothalamus. Somata size measurements were taken for AGRP, NPY, and pomc1a from the NLTv, NLTi, and NLTm throughout the rostro-caudal extent shown. Left side shows cresyl violet stained section and right side shows traced nuclei. Scale bars (A-D) = 250 µm. Approximate location of each transverse section is indicated on E. Hypothalamic tissue (shaded gray in E) used for qPCR analysis was macro-dissected via cuts (lines) at the locations indicated on the sagittal brain illustration shown in E. See list for abbreviations.

181x135mm (300 x 300 DPI)

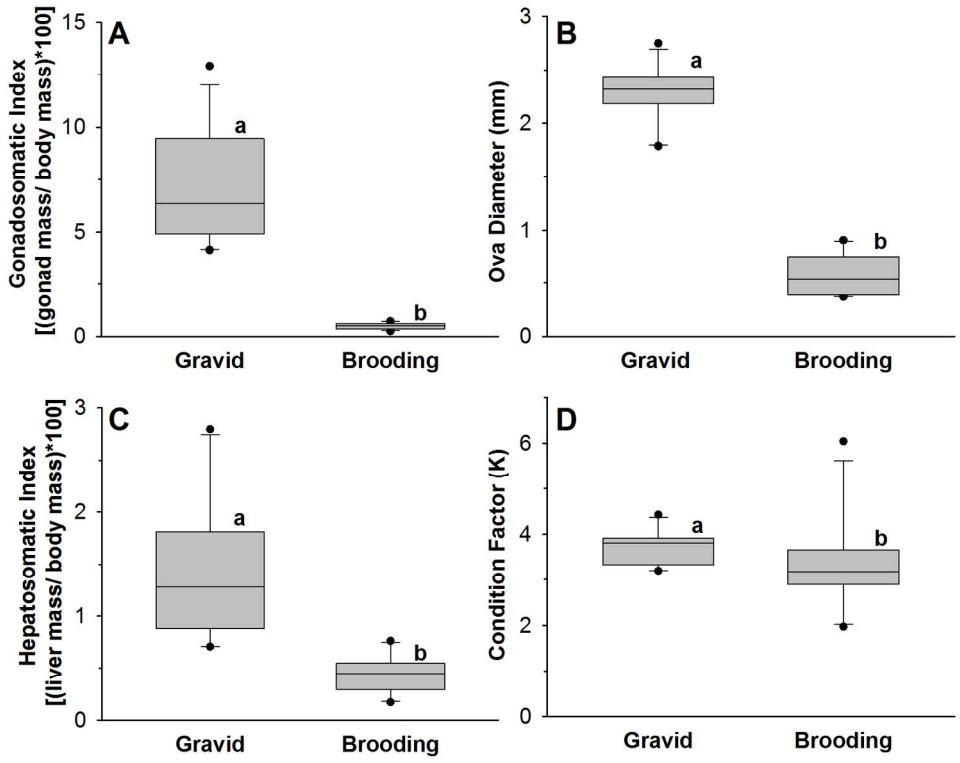

Figure 4. Physiological differences between gravid and mouth brooding Astatotilapia burtoni females. Gravid females have greater gonadosomatic index (GSI) (A), ova diameters (B), hepatosomatic index (HSI) (C), and condition factors (D) compared to brooding females. In each graph, the bottom of each box is the 25th percentile, the top is the 75th percentile and the line in the middle is the median. Whiskers (error bars) indicate the 10th and 90th percentiles and dots represent points outside the 10th-90th percentile. N=12 for both gravid and brooding females for A-D. Different letters indicate statistical differences at $p<0.05$.

160x128mm (300 x 300 DPI)

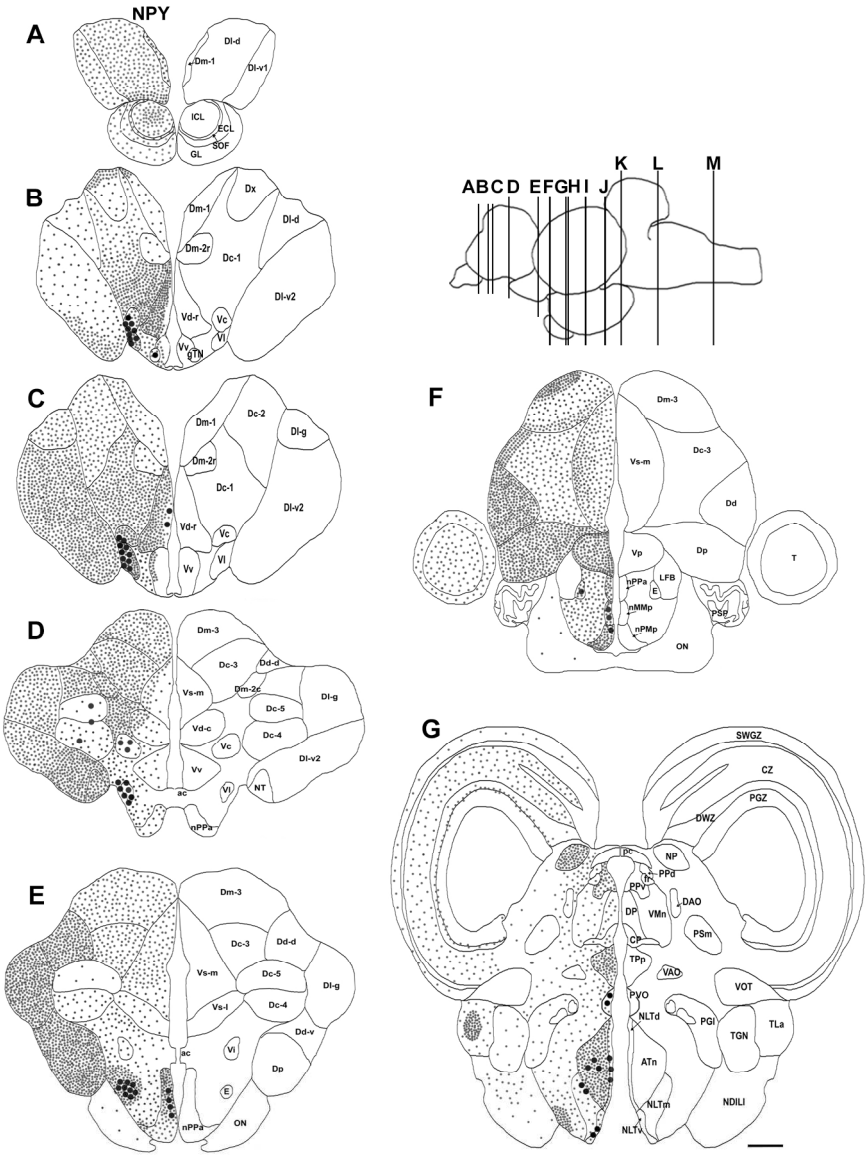

Figure 5. Localization of neuropeptide Y (NPY)-immunoreactive neurons in the brain of Astatotilapia burtoni. Representative line drawings of transverse sections from rostral (A) to caudal (N) brain regions show the locations of NPY ir-somata (large black dots) and fibers (small black dots). Left side of brain shows NPY distribution and right side shows labels of nuclei and other neuroanatomical structures. Figure inset at the top right shows a lateral view of the brain indicating the approximate location of each transverse section. Scale bar = 250 μm. See list for abbreviations.

171x230mm (300 x 300 DPI)

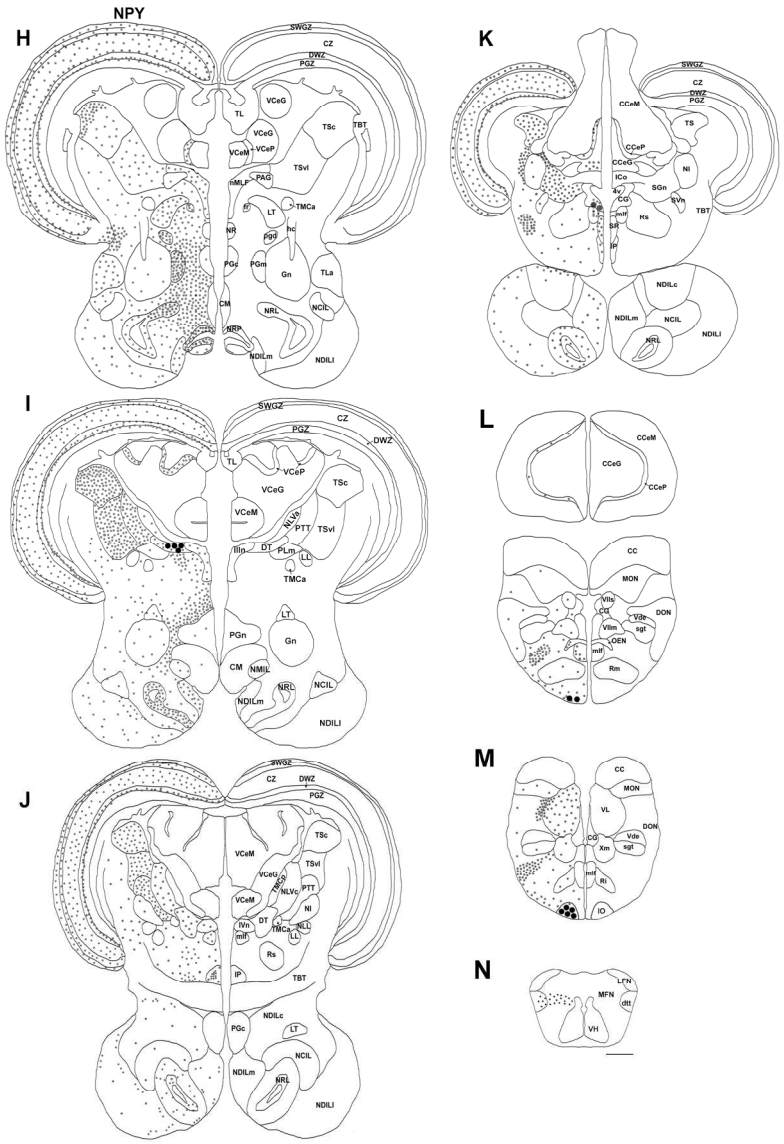

Figure 5. Localization of neuropeptide Y (NPY)-immunoreactive neurons in the brain of Astatotilapia burtoni. Representative line drawings of transverse sections from rostral (A) to caudal (N) brain regions show the locations of NPY ir-somata (large black dots) and fibers (small black dots). Left side of brain shows NPY distribution and right side shows labels of nuclei and other neuroanatomical structures. Figure inset at the top right shows a lateral view of the brain indicating the approximate location of each transverse section. Scale bar = 250 μm. See list for abbreviations.

171x230mm (300 x 300 DPI)

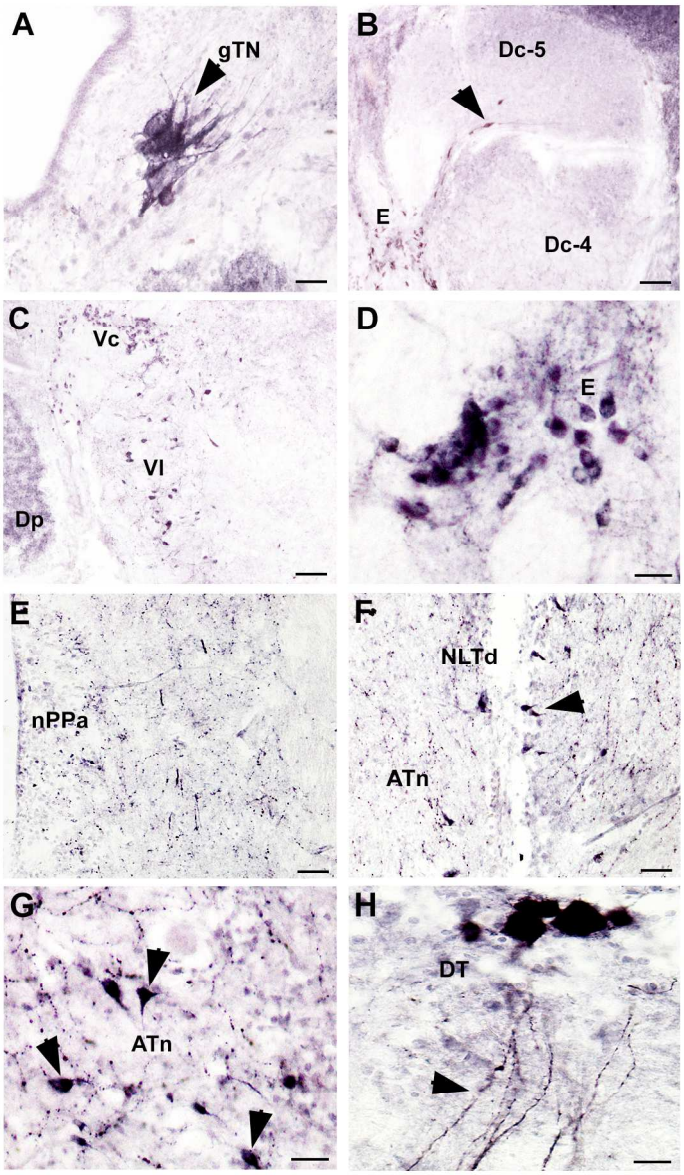

Figure 6. Representative photomicrographs of NPY-immunoreactive somata and fibers in the brain of Astatotilapia burtoni. Coronal sections showing NPY-ir cells in gTN (A). NPY-ir cells in the region between Dc-4 and Dc-5 (arrowhead) (B). Cells and fibers in the Vc and VI (C) and entopeduncular nucleus (D). NPY-ir fibers in the nPPa (E). In the diencephalon, NPY-ir cells and fibers are found in the ATn and NLTd of the hypothalamus (arrowheads) (F-G). Large NPY-ir cells in DT and ventrally projecting varicose fibers (arrowhead) (H). Scale bars = 50 μm B, C; 25 μm in A, E, F; 10 μm in D, G, H. See list for abbreviations.

171x230mm (300 x 300 DPI)

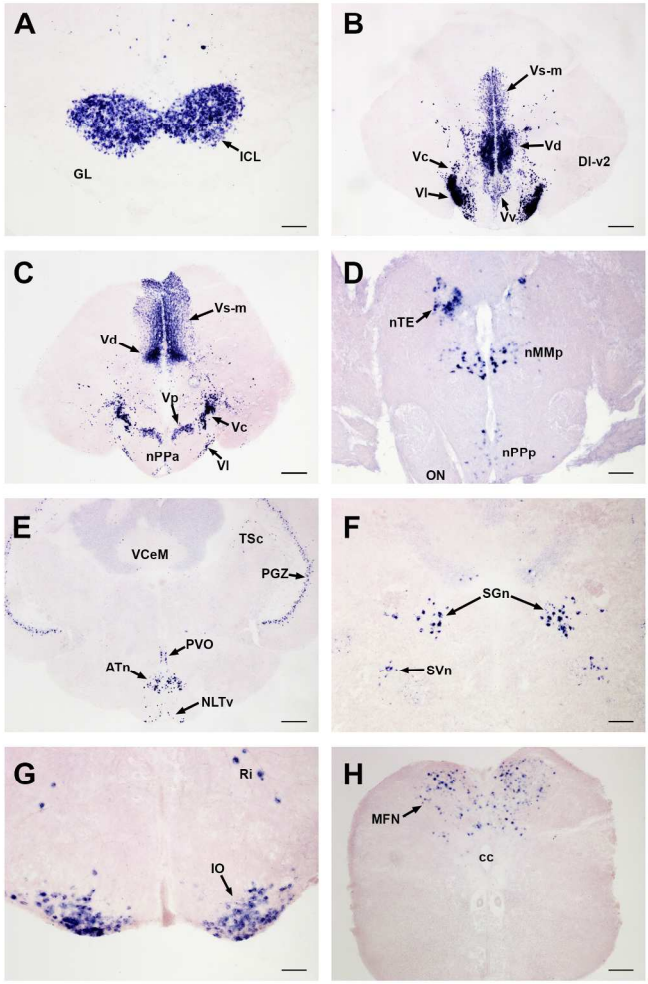

Figure 7. Representative photomicrographs of npy–expressing cells in the brain of Astatotilapia burtoni. Cells are abundant in the ICL of the olfactory bulb (A), and in subpallial nuclei of the ventral telencephalon, including Vv, Vl, Vc, Vd, Vs-m, and Vp (B-C). npy cells also lie in preoptic nuclei nPPa, nPPp, and nMMp, as well as nTE (C-D). Cells lie in the PVO, ATn, and NLTv regions, as well as the PGZ of the tectum, and TSc (E). In the rhombencephalon, npy-expressing cells are found in the SGn, SVn, IO, Ri, and MFN of the rostral spinal cord (F-H). Scale bars = 100 μm (A, D, F, H), 250 μm (B, C, E), 50 μm (G).

203x254mm (300 x 300 DPI)

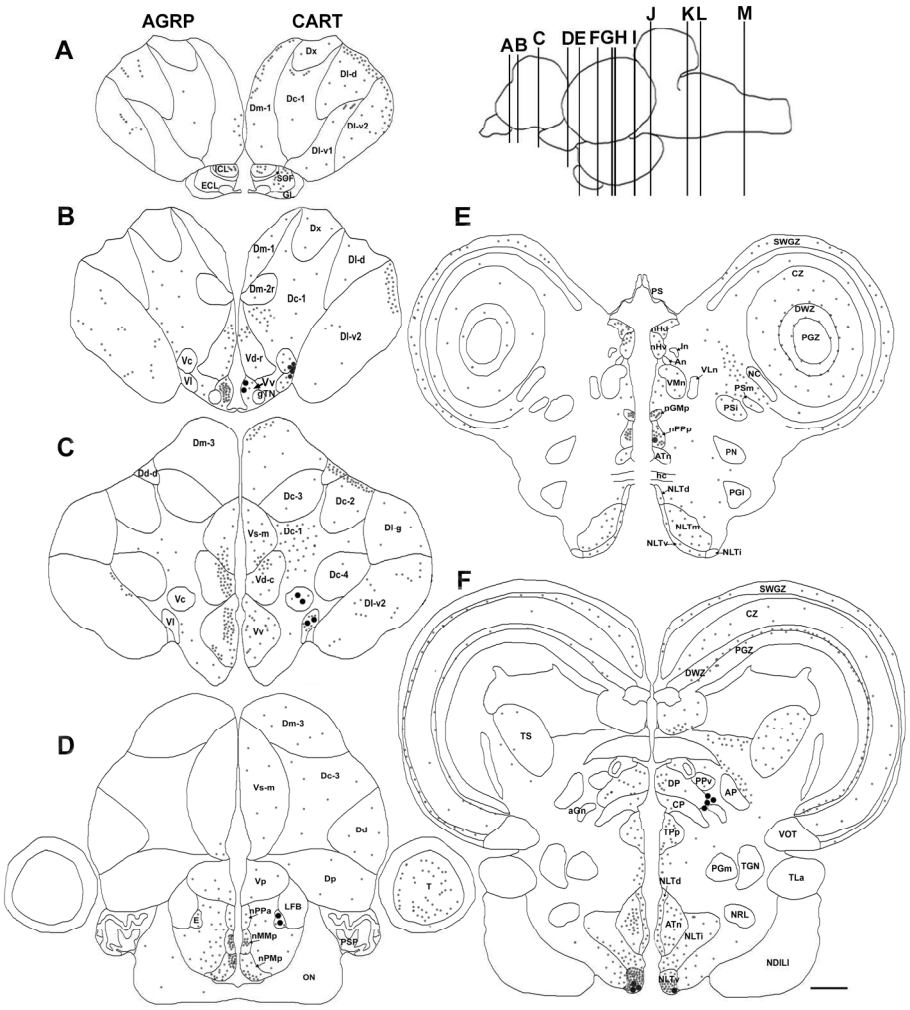

Figure 8. Localization of AGRP (left half)- and CART (right half)-immunoreactivity in the brain of Astatotilapia burtoni. Representative line drawings of transverse sections from rostral (A) to caudal (M) brain regions show the locations of AGRP and CART ir-somata (large black dots) and fibers (small black dots). Left side of brain shows AGRP distribution and right side shows CART distribution, along with labels of nuclei and other neuroanatomical structures. Figure inset at the top right shows a lateral view of the brain indicating the approximate levels of the corresponding transverse sections. Scale bar = 250 μm. See list for abbreviations.

190x230mm (300 x 300 DPI)

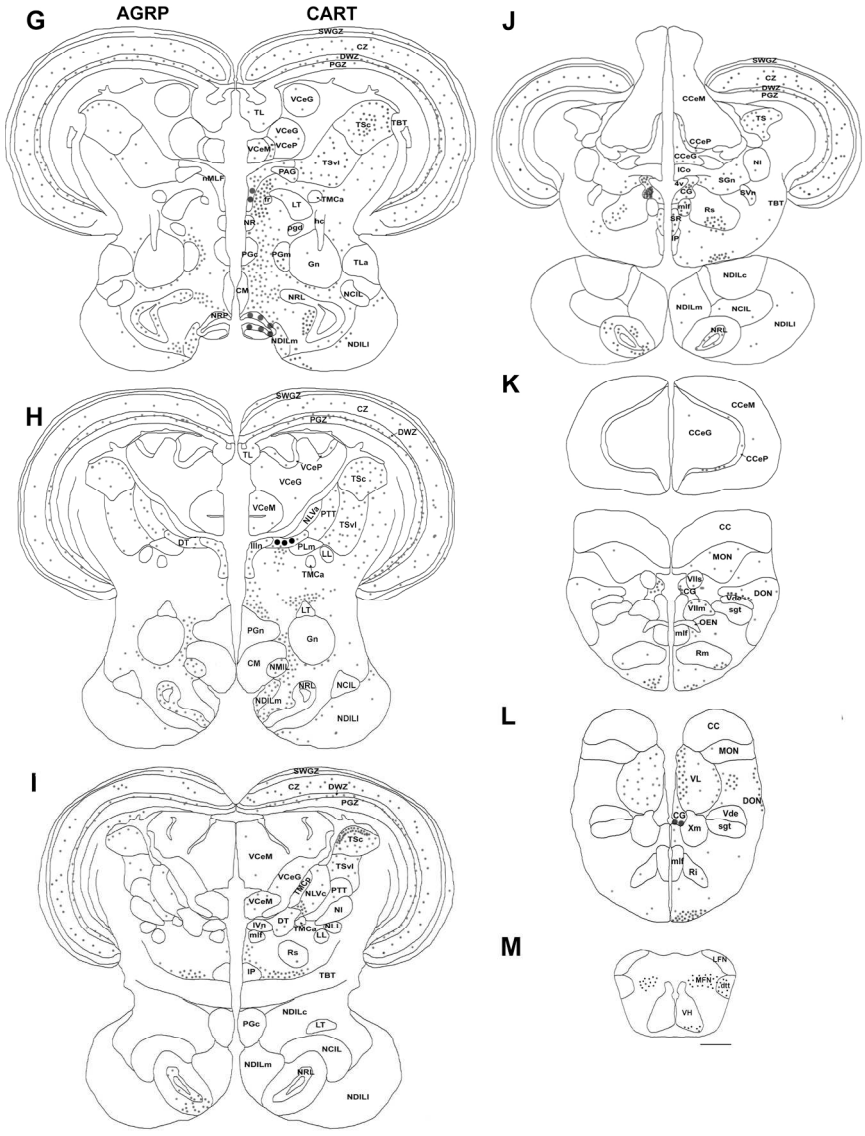

Figure 8. Localization of AGRP (left half)- and CART (right half)-immunoreactivity in the brain of Astatotilapia burtoni. Representative line drawings of transverse sections from rostral (A) to caudal (M) brain regions show the locations of AGRP and CART ir-somata (large black dots) and fibers (small black dots). Left side of brain shows AGRP distribution and right side shows CART distribution, along with labels of nuclei and other neuroanatomical structures. Figure inset at the top right shows a lateral view of the brain indicating the approximate levels of the corresponding transverse sections. Scale bar = 250 µm. See list for abbreviations.

171x230mm (300 x 300 DPI)

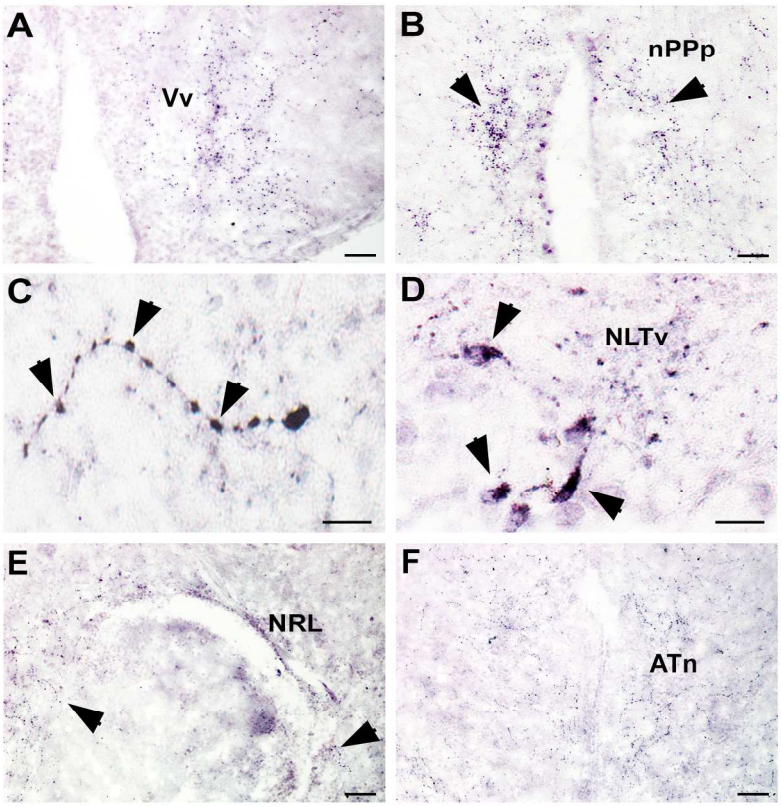

Figure 9. Representative photomicrographs of AGRP-immunoreactive somata and fibers in the brain of Astatotilapia burtoni. Coronal sections of the diencephalon show immunoreactive fibers in Vv (A). Moderately dense fibers (arrowheads) in nPPp (B). Immunoreactive fibers with large varicosities (arrowheads) in NLTv of the hypothalamus (C). AGRP-ir cells (arrowheads) and fibers in NLTv (D). Scattered fibers (arrowheads) are present in the NRL surrounding the lateral recess (E), and in the ATn (F). Scale bars = 25 μm in A, B, E; 10 μm in C, D; 50 μm in F. See list for abbreviations.

171x230mm (300 x 300 DPI)

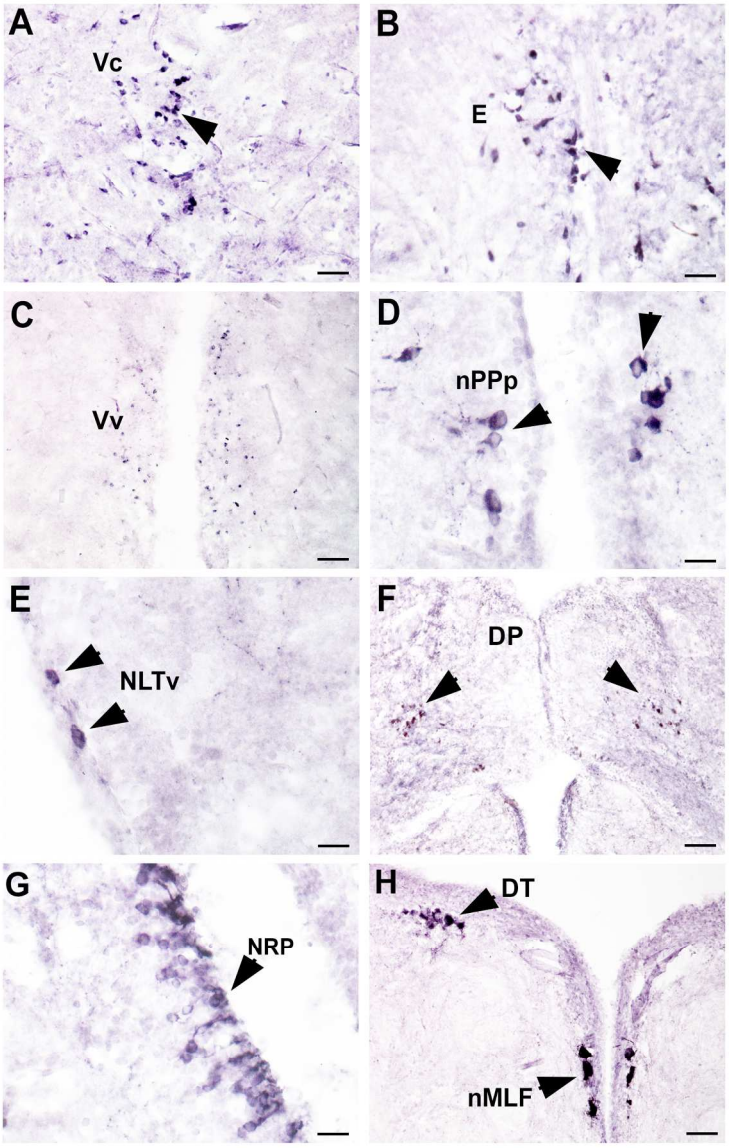

Figure 10. Representative photomicrographs of CART-immunoreactive somata and fibers in the brain of Astatotilapia burtoni. Coronal sections of the telencephalon show CART-ir cells (arrowheads) in the Vc (A) and entopeduncular nucleus (B). Small CART-ir cells in Vv (C). Immunoreactive cells (arrowheads) in the nPPp (D) and NLTv (E). A group of small CART-ir cells lies in the thalamus adjacent to DP (F). CART-ir cells in NRP (G). Large immunoreactive cells are also present in DT and along the midline in nMLF (H) of the mesencephalon. Scale bars = 25 μm in A, B, D; 50 μm in C, F, H; 10 μm in G, E. See list for abbreviations.

171x230mm (300 x 300 DPI)

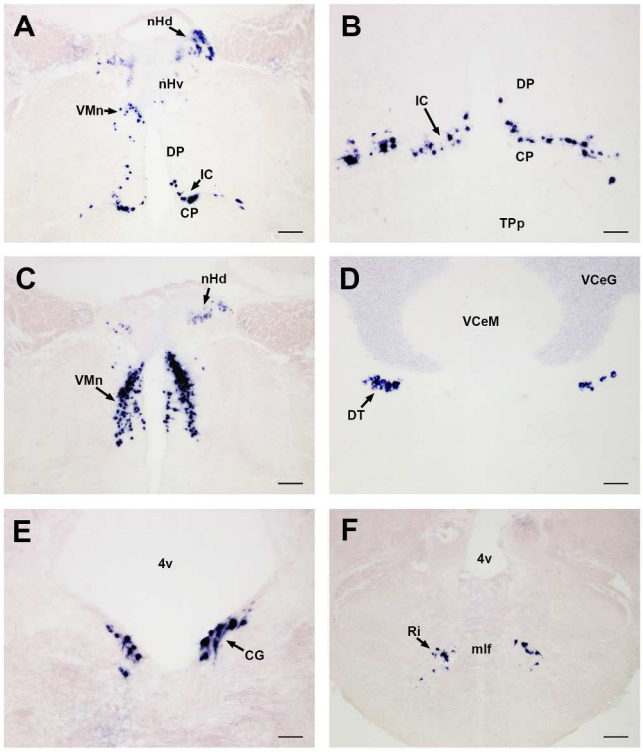

Figure 11. Representative photomicrographs of cart4–expressing cells in the brain of Astatotilapia burtoni. cart4 cells in the habenula (nHd), and thalamic VMn and IC (A-C). Cluster of large cells in DT (D). In the hindbrain, cart4 cells are found in the CG and Ri (E-F). Scale bars = 100 μm (A, C, D, F), 50 μm (B, E).

203x254mm (300 x 300 DPI)

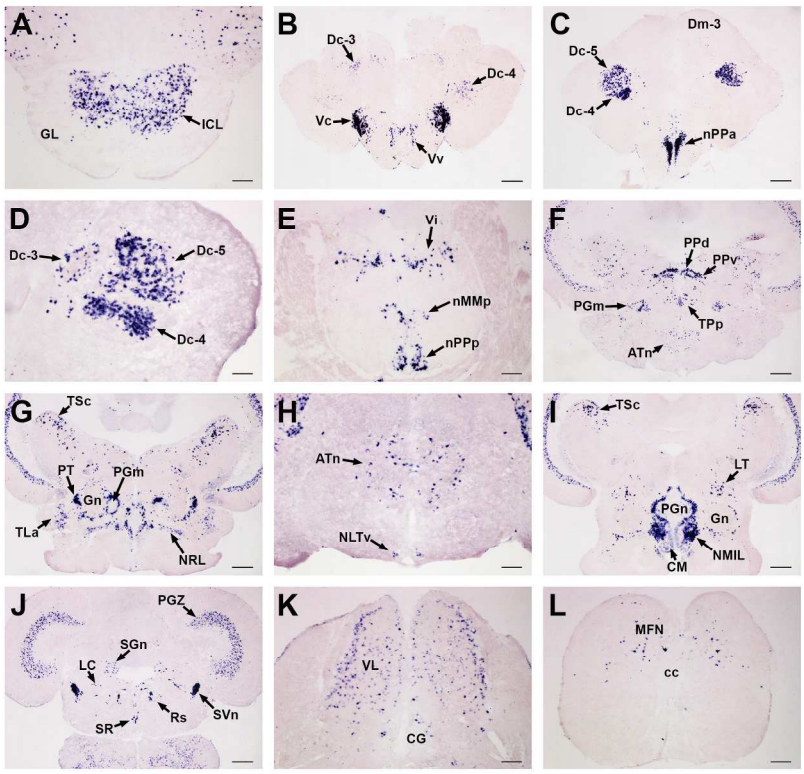

Figure 12. Representative photomicrographs of cart2–expressing cells in the brain of Astatotilapia burtoni. cart2-expressing cells are abundant in the ICL of the olfactory bulb (A). In the telencephalon, numerous cart2 cells lie in subpallial Vc/Vl, Vv, and Vi regions, as well as pallial Dc-3, -4, and -5 (B-E). cart2 cells are expressed in preoptic nuclei nPPa, nPPp, and nMMp (C,E). cart2 cells in the PPd, PPv, TPp, ATn, and PGm (F). Cells lie in several diencephalic and mesencephalic regions, including PT, TLa, TSc, and NRL, and cells surround some nuclei such as PGm (G). The ATn and NLTv have cart2-expressing cells (H). Cells lie in TSc, LT, CM, and NMIL, and cells surround Gn and PGn (I). cart2 cells also lie in the PGZ of the tectum, SGn, SVn, LC, SR, and Rs (J). In the rhombencephalon, cart2-expressing cells are found in the sensory vagal lobe (VL) and MFN of the rostral spinal cord (K-L). Scale bars = 100 μm (A, D, E, H, K, L), 250 μm (B, C, F, G, I, J).

203x254mm (300 x 300 DPI)

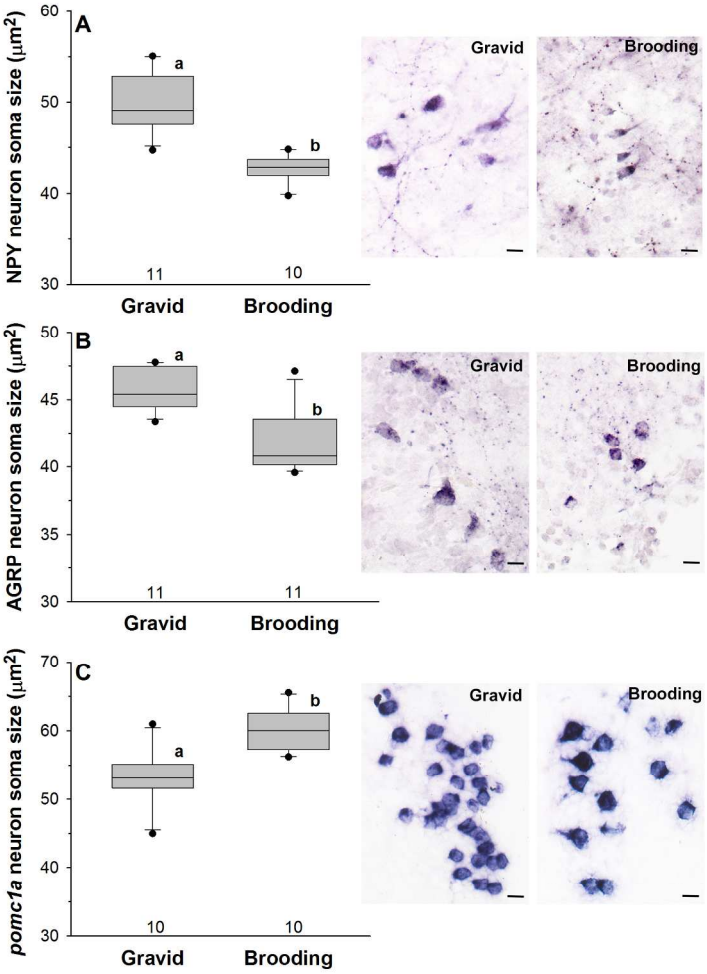

Figure 13. Reproductive state differences in somata sizes of AGRP, NPY, and pomc1a neurons in the lateral tuberal nucleus of Astatotilapia burtoni females. NPY-ir (A) and AGRP-ir (B) somata sizes are larger in gravid compared to brooding females, while pomc1a (C) neurons are larger in brooding compared to gravid females. In each graph, the bottom of each box is the 25th percentile, the top is the 75th percentile and the line in the middle is the median. Whiskers (error bars) indicate the 10th and 90th percentiles and dots represent points outside the 10th-90th percentile. Sample sizes (number of fish analyzed) are indicated beneath each plot. Different letters indicate statistical differences at $p<0.05$. Representative stained transverse sections through the NLT for gravid and brooding females are shown at right. Scale bars = 10 μm.

203x254mm (300 x 300 DPI)

Porter et al.

Graphical abstract text

Immunohistochemistry, *in situ* hybridization, and quantitative PCR were used to describe the localization of anorexigenic (cocaine and amphetamine-regulated transcript, CART; pro-opiomelanocortin, pomc) and orexigenic (neuropeptide Y, NPY; agouti-related protein, AgRP) neurons in the cichlid brain, and to demonstrate differences in neuron somata sizes between females of different reproductive and metabolic states.

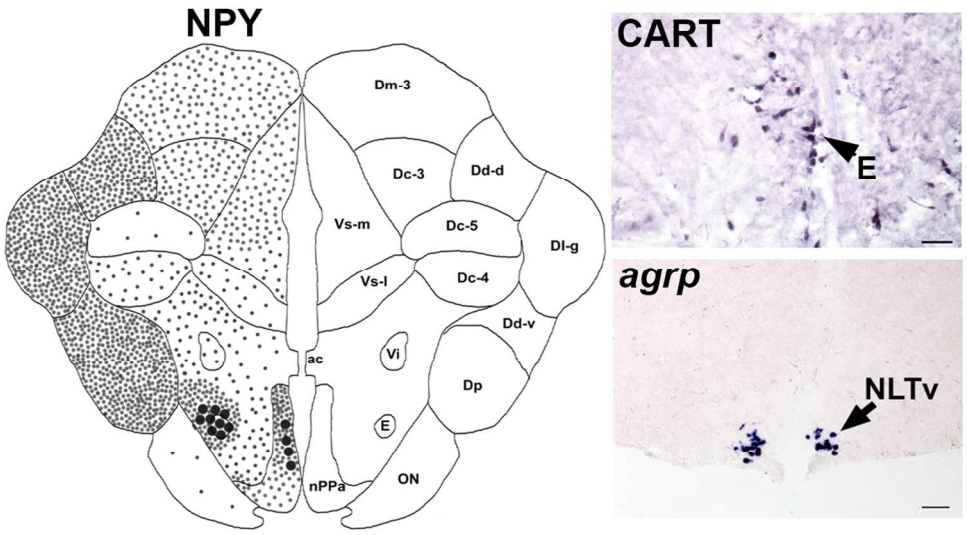

112x61mm (300 x 300 DPI)